Applied Thermal Engineering 246 (2024) 122940

Contents lists available at ScienceDirect

Applied Thermal Engineering

journal homepage: www.elsevier.com/locate/apthermeng

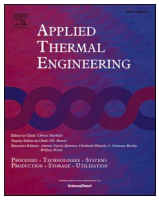

Research Paper

Variable valve actuation for efficient exhaust thermal management in an off-road diesel engine

Jeyoung Kim [a,*], Marko Vallinmaki [b], Tino Tuominen [c], Maciej Mikulski [a]

[a] University of Vaasa, School of Technology and Innovations, Efficient Powertrain Solutions (EPS) research group, Wolffintie 32, FI-65200 Vaasa, Finland
[b] AGCO Power, Linnavuorentie 8-10, FI-37240 Linnavuori, Finland
[c] VTT Technical Research Centre of Finland, PL 1000, 02044, Espoo, Finland

ARTICLE INFO

Keywords:
VVA
After-treatment thermal management
Predictive combustion model
Diesel combustion
Emissions
Off-road diesel engines

ABSTRACT

Exhaust thermal management (ETM) is crucial for effective emission mitigation in integrated exhaust after-treatment systems of modern off-road diesel powertrains. However, conventional ETM strategies incur a significant fuel efficiency penalty. This study addresses the issue by investigating the application of variable valve actuation (VVA) for efficient ETM. For the first time, this investigation is conducted on a representative state-of-the-art off-road powertrain platform. It explores four VVA strategies with unprecedent level of rigour, employing a model-based approach that enables extended insights beyond stand-alone testing. Experiments with an EU Stage-V off-road diesel engine provide the baseline for validating a one-dimensional model in GT-Suite. A meticulously calibrated, predictive combustion model enables precise cross-evaluation of how VVA strategies affect exhaust gas temperature (EGT), efficiency, engine-out emissions and combustion characteristics, considering all trade-offs. VVA simulations are performed at three low-load operating points, where engine operation borders catalyst light-off temperature (LOT). The findings impartially confirm that cylinder deactivation (CDA) and intake modulation are the most promising VVA strategies for off-road engines, with EGT increments surpassing +250 °C and +150 °C respectively, accompanied by minor fuel penalties (up to +3.5 %). CDA demonstrated fuel savings of up to −2.5 % at certain points, due to reduced pumping and friction losses. Intake modulation displayed large reduction in engine-out NO_x (>90 %) and minimal penalties in carbon emissions (HC, CO, and soot). The results underscore VVÁs potential as an efficient ETM option to help the next generation of off-road diesels to comply with upcoming EPA Tier 5 emission legislation.

1. Introduction

Compression ignition (CI) will remain dominant for heavy-duty (HD) off-road applications for the foreseeable future. High energy density of the fuel, combined with good thermal efficiency and robustness, support this status quo [1]. Although the on-road sector has made rapid progress towards electrification, the low power density of Li-ion batteries means this roadmap is not fully feasible for the off-road sector [2]. Hybridisation offers additional advantages through a variety of energy- and thermal-management strategies. Furthermore, low-carbon renewable fuels provide an immediate route towards decarbonisation in energy-demanding applications. Therefore, it is important to implement effective exhaust aftertreatment systems (EATS) and exhaust thermal management (ETM) to achieve net-zero emissions in CI engines.

Despite their merits, CI engines are notorious for their emissions of harmful air pollutants, particularly nitrogen oxides (NO_x) and particulate matter (PM) due to the presence of both locally fuel-rich zone and high flame temperature [1,3]. High-pressure multiple injection [4,5] and exhaust gas recirculation (EGR) [6] were developed to address these issues. However, relying solely on in-cylinder emission control strategies proves inadequate for simultaneously reducing both emissions due to the inherent trade-off between NO_x and PM in conventional CI engines. Consequently, the adoption of EATS has become necessary to ensure compliance with the increasingly stringent emission regulations in off-road applications, such as EU Stage-V or US EPA Tier 4 final limits.

Contemporary EATS is heavily integrated, as illustrated in Fig. 1. A diesel oxidation catalyst (DOC) reduces hydrocarbon (HC), carbon monoxide (CO), and soluble organic fraction through catalytic reactions with oxygen [7,8]. Subsequently, a diesel particulate filter (DPF) captures PM via filtration. Additionally, selective catalytic reduction (SCR) technology addresses NO_x through reaction with urea. The urea is

* Corresponding author.
E-mail address: jeyoung.kim@uwasa.fi (J. Kim).

https://doi.org/10.1016/j.applthermaleng.2024.122940
Received 10 January 2024; Received in revised form 6 March 2024; Accepted 12 March 2024
Available online 13 March 2024

Nomenclature

Abbreviations

1D	one-dimensional
2EVO	secondary exhaust valve opening
2IVO	secondary intake valve opening
AFR	air–fuel ratio
AOC	ammonia oxidation catalyst
AVG	average values
BDC	bottom dead centre
BMEP	brake mean effective pressure
BSFC	brake specific fuel consumption
$BSNO_x$	brake specific nitrogen oxides (g/kWh)
CAC	charge-air cooler
CAD	crank angle degree
CCO	cylinder cut-out
CDA	cylinder deactivation
CHR	cumulative heat release
CI	compression ignition
CO	carbon monoxide
DOC	diesel oxidation catalyst
DPF	diesel particulate filter
EATS	exhaust aftertreatment systems
ECU	engine control unit
EEVO	early exhaust valve opening
EGR	exhaust gas recirculation
EGT	exhaust gas temperature
EIVC	early intake valve closing
ETM	exhaust thermal management
EVC	exhaust valve closing
EVO	exhaust valve opening
FS	full scale
HC	hydrocarbon
HD	heavy-duty
HRR	heat release rate
IAF	intake air mass flow
IMEP	indicated mean effective pressure
$IMEP_g$	gross indicated mean effective pressure
$IMEP_n$	net indicated mean effective pressure
IVC	intake valve closing
IVO	intake valve opening
LEVO	late exhaust valve opening
LIVC	late intake valve closing
LOT	light-off temperature
MFB	mass fraction burned
NO_x	nitrogen oxides
NRTC	non-road transient cycle
NVO	negative valve overlap
OP	operating point
PM	particulate matter
PMEP	pumping mean effective pressure
PN	particle number
RGF	residual gas fraction
SCR	selective catalytic reduction
SOI	start of injection
TDC	top dead centre
VGT	variable geometry turbine
VVA	variable valve actuation

decomposed into NH_3, through hydrolysis and thermolysis, where NH_3 serves as a reductant in the SCR [9]. Higher urea concentration in the catalyst results in greater NO_x reduction, yet it is crucial to recognize that not all ammonia (NH_3) is absorbed by the catalyst surface, with excess being released into the exhaust stream [9,10]. Consequently, precise control of urea injection is imperative [9]. Alternatively, an ammonia oxidation catalyst (AOC) may be incorporated to manage ammonia slips from the SCR. Although modern diesel engines primarily emit NO_x in the form of NO [11], this is converted to NO_2 in the DOC and SCR [11]. The conversion of NO to NO_2 impacts both DPF passive regeneration [12] and NO_x reduction in the SCR [8]. Nevertheless, the adoption of EATS introduces inherent challenges, including higher vehicle costs for consumers, increased backpressure in the exhaust system, additional maintenance requirements and the periodic need to replenish the urea reservoir [13].

Regulation can influence the configuration of integrated EATS. For example, EPA Tier 4 final regulations in North America do not restrict the number of particulate matters (PN-particle number), so DPFs are less common [14]. Instead, the EPA regulation focus on enhancing the effectiveness of DOCs to address emissions concerns [14]. Conversely, DPFs are becoming widespread in Europe to comply with new restriction of particle number (PN) in EU Stage-V regulations.

Contemporary EATS demonstrate excellent performance. López et al. [15] tested a state-of-the-art, vanadium-based SCR catalyst on a US2007, 8.9-litre diesel engine and achieved NO_x conversion efficiency of up to 92 % during non-road transient cycle (NRTC) tests. Higher conversion efficiency is achievable with dual-dosing, double SCR systems [16,17] or by adopting a pre-turbine layout [18,19]. The modern DOC can remove up to 90 % of unburned HC and as much as 99 % of CO at high exhaust gas temperature (EGT) [20]. Hu et al. [21] implemented DOC, catalytic DPF and SCR for a non-road diesel engine, demonstrating an average reduction of more than 90 % in emissions of CO, HC, NO_x, PN, and PM in non-road steady cycle test. However, it was reported that the performance of EATS diminishes notably when EGT is relatively low.

Feng et al. [22] further examined the effect of exhaust gas thermal conditions on emissions in a non-road diesel engine by analysing experimental results of hot and cold NRTC tests. EATS consisted of DOC, partial oxidation catalyst, SCR, and AOC. Low EGT in the cold cycle attributed to lower conversion efficiency. Specifically, PM conversion efficiency decreased by 31 % compared to the hot cycle, exceeding China-IV PM standards. Notably, it took approximately 400 ~ 500 s for the SCR catalyst temperature to attain 200 °C in the NRTC cold mode [14]. This time constitutes one-third of the entire mode duration, so it exerted a substantial influence on NO_x emissions. Consequently, NO_x, HC, CO, and CO_2 exhibited markedly lower conversion efficiencies during the early stage (0–600 s) of the cold NRTC mode.

EGT is one of crucial factors, along with exhaust mass flow rate and exhaust gas composition, to influence the performance of DOC and SCR

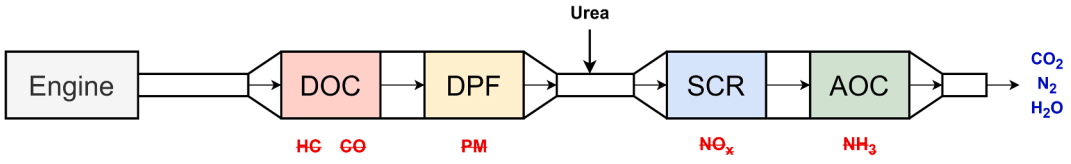

Fig. 1. Modern integrated exhaust aftertreatment system for diesel engines.

[8,22]. High EGT accelerates catalytic reactions, providing high EATS conversion efficiency. High EGT also is beneficial for DPF regeneration [23]. Conversely, low EGT slows catalytic reactions, resulting in poor performance of the DOC and SCR system. The light-off temperature (LOT) - the temperature at which conversion efficiency reaches 50 % - is normally used to indicate the effectiveness of the catalyst.

The LOT varies over each application by catalyst metal composition, space velocity, exhaust gas composition and design of the aftertreatment brick [20]. Guardiola et al. [8] noted that various emission species exhibit distinct LOTs, with HC and CO having LOTs of 190 °C and 150 °C, respectively. Furthermore, DOC ageing increased the LOT of HC and CO to 250 °C and 205 °C respectively, but catalytic monolith length of the DOC showed no significant effect on LOT. Guardiola et al. [24] and Tharad [25] reported that the LOT of the modern DOC is 200 °C. According to Villamaina et al. [26] and Ma et al. [27], the LOT of an SCR system is 170 °C – 270 °C with different catalyst compositions. Additionally, the SCR system requires a temperature above 200 °C to decompose urea and thus avoid solid deposits [28]. Despite some variations in these temperature ranges, Vos et al. [29] and Ko et al. [11] claimed that EATS necessitates catalyst temperatures exceeding 250 °C to 300 °C for effective emission mitigation.

Reaching this threshold can be challenging in real world operation, particularly during the cold-start, warm-up phase and when idling. EGT can be as low as 100 °C when an engine is idling [30,31]. Lauren et al. [32] and Magee [33] consistently reported that EGT remains below 250 °C when engine load is lower than 30 % in contemporary off-road and on-road diesel engines. Various ETM techniques can be used to satisfy the increasing demand for high EGT over a wider range of operating conditions. To this end, most production engines already incorporate either intake or exhaust throttling. These slow-response, airpath-based ETM measures can be combined with fast in-cylinder thermal management via late post injection.

Bai et al. [30] demonstrated an EGT greater than 200 °C at low load (3 % load) using intake throttling in a 7-litre, HD diesel engine. Lauren et al. [32] evaluated intake and exhaust throttling in off-road diesel engines, raising EGT by more than 200 °C. Both studies observed that excessive throttling could raise EGT, but that this approach leads to poor gas exchange process since the airpath is highly restricted. The two studies reported high penalties of break specific fuel consumption (BSFC), of up to 14.3 % and 20 % respectively. Wu et al. [34] employed a late post injection strategy on a six-cylinder, HD diesel engine, showing that EGT was increased by delaying post injection timing and increasing post injection quantity. In the end, EGT was increased by about 60 °C, but accompanied by a 3.4 % reduction in the brake thermal efficiency. Gosala et al. [1] implemented exhaust throttling in a HD diesel engine via an over-closed variable geometry turbine (VGT) vane, coupled with late post injection. Fuel efficiency deteriorated by up to 58 % at idling condition, while EGT increased by around +115 °C.

It is evident from the above reviews that there is a trade-off between EGT increment and fuel efficiency. Traditional ETM strategies demonstrate a significant fuel penalty that is deemed unacceptable in an off-road sector which values high fuel efficiency. Variable valve actuation (VVA) offers a more promising solution by mimicking the throttling effect of ETM while mitigating the trade-off with efficiency.

Conventionally, VVA has been widely implemented in spark-ignition engines to improve volumetric efficiency and engine performance over a wide operating envelope. However, VVA is subjected to more rigorous mechanical constraints in diesel engines. Their high compression ratio means the clearance between piston and cylinder head at the top dead centre (TDC) is relatively small. This prohibits deep valve pockets on the piston surface and allows only a small margin for advancing intake valve opening (IVO) and retarding exhaust valve opening (EVO) [35,36]. Consequently, production diesel engines have shown only limited VVA applications, such as Miller timing, addressed through a mechanical cam-based partial or two-step VVA system.

However, an advanced, fully flexible, cam-less VVA system could provide more control beyond mechanical limitations. For example, it could control all valves independently at each cylinder. This would enable sophisticated VVA strategies such as asymmetric valve opening or cylinder deactivation (CDA), as well as more precise cycle-to-cycle or cylinder-to-cylinder control [37]. This could improve gas exchange, combustion stability, emissions and thermal management. Nevertheless, cam-less valvetrains face challenges, including precise and robust control, potentially increased parasitic losses and complexity of VVA calibration [38]. Multiple engine performance benefits need to be proven before moving this technology from proof of concept to the production stage.

Table 1 collates the most relevant, up-to-date research involving VVA for HD diesel engine ETM. The discussion includes only a very brief account of the individual contributions, but a more detailed analysis of the subject can be found in a review article by Kim et al. [39]. Table 1 shows that various studies have demonstrated that VVA is capable of increasing EGT in HD diesel engines. Intake valve modulation, such as early intake valve closing (EIVC) and late intake valve closing (LIVC) is by far the most researched technique. It is relatively easy to implement by a mechanical, cam-driven partial VVA system, and has been realised as Miller timing for effective in-cylinder NO_x reduction. Gehrke et al. [40] investigated advanced and retarded IVC timing. These raised EGT by up to +58 °C and +116 °C respectively, with minor BSFC deterioration (<2.6 %). Guan et al. [41] applied LIVC and raised EGT increment by up to +52 °C, with a BSFC penalty of +5.3 %. Ojeda [42] demonstrated EIVC and elevated EGT by up to +90 °C, while also improving fuel efficiency by 4.5 %.

Table 1 reveals large variations in fuel penalty and EGT increment between individual studies, even in the same VVA category. For instance, Gehrke et al. [40] and Guan et al. [41] reported a negative impact on BSFC, while Ojeda [42] observed a positive impact on fuel efficiency in EIVC and LIVC. Vos et al. [29] indicated minor fuel benefit (−1.5 %) in CDA, but Magee [33] reported a BSFC improvement of up to −10 %, with similar EGT increment. Zhang et al. [43] observed better BSFC by −1.2 % in secondary intake valve opening (2IVO), while Wickström [44] reported a BSFC penalty of up to +9 %. Apart from EGT and BSFC penalty, the majority of the studies included analysis on how VVA strategies affected emissions. Once again, similar VVA strategies produced inconsistent emission trends. In LIVC, Gehrke et al. [40] indicated PM up by 234 % and constant NO_x, while Guan et al. [41] reported NO_x decreased by 13.5 % and PM down by 81 %. In secondary exhaust valve opening (2EVO), Joshi et al. [45] achieved NO_x reduction of 80 %, while Zhang et al. [43] reported a constant NO_x level.

The above discussion highlights the conflicting results between works covering similar VVA strategies on different operating platforms and at different operating points. The effectiveness of each VVA strategy is strongly influenced by the engine-specific valve profiles, injection parameters, emission control strategy, calibration, etc. Backpressure level in the exhaust can vary between positive and negative, which will impose opposite effects on in-cylinder backflows. This huge span of cross-dependencies makes it impossible to use these results to assess whether VVA is a suitable next development step for off-road engines.

Furthermore, most of the relevant works that provide reliable experimental results on VVA effects are technical papers, and so provide limited insight into the mechanisms underpinning the demonstrated performance/emission results. Most of the VVA strategies considered in Table 1, aside from their direct impact on ETM and pumping work, involve a feedback loop to combustion and emission formation, through changes to in-cylinder trapped mass/ratio of residuals. Sole multi-cylinder engine experiments are not enough to thoroughly characterise the phenomena related to VVA-ETM, implying the significance of predictive models as supporting tools.

The present study aims to address the above knowledge gaps by utilizing a cutting-edge, EU Stage-V compliant off-road diesel engine as the baseline for a comprehensive simulation of all available VVA strategies. A well-validated predictive combustion model enables accurate

Table 1
Summary of the most relevant research works concerning the use of VVA for efficient ETM.

Ref	Type of Engine	VVA strategy	Operating conditions	Results			
			Speed / load	ΔEGT	ΔBSFC	ΔNOx	ΔPM or Soot
			[RPM] / [bar]	[℃]	[%]	[%]	[%]
Gehrke et al. (2013) [40]	HD diesel engine, 1.6L, single-cylinder	EIVC	1250 / 5.4 (BMEP)	+58	+1.2	0	+104
		LIVC		+116	+2.6	0	+234
Guan et al. (2019) [41]	HD diesel engine, 2.0L, single-cylinder, EGR	LIVC	1150 / 2.2 (BMEP)	+52	+5.3	−13.5	−81
Ojeda (2010) [42]	HD diesel engine, 6.4L, eight-cylinder HP*-EGR	EIVC	2050 / 4.3 (BMEP)	+90	−4.5	0	−66
Joshi et al. (2022) [45]	HD diesel engine, six-cylinder, HP*-EGR, VGT	2EVO	800 / 1.3 (BMEP)	+52	+3	−80	+300
Wickström (2012) [44]	HD diesel engine, 2.0L, single-cylinder	2IVO	1200 / 25 % load	+144	+9	−81	> 2.5 FSN*
Zhang et al. (2016) [43]	HD diesel engine, 1L, single-cylinder	2EVO	– / 1.3 (IMEP)	+78	−1.6	0	> 0.1 FSN*
		2IVO		+55	−1.2	−39	< 0.04 FSN*
Vos et al. (2021) [29]	HD diesel engine, six-cylinder, HP*-EGR, VGT	CDA	2200 / 3.9 (BMEP)	+117	−1.5	+4	+19
Magee (2014) [33]	HD diesel engine, 6.7L, six-cylinder, HP*-EGR, VGT	CDA	1200 / 13 % load	+100	−10	NA	NA

ΔEGT (+: increased temperature; –: decreased temperature) ΔBSFC (+: deteriorated or increased fuel consumption; –: improved or reduced fuel consumption). ΔNO_x / ΔPM or Soot (+: deteriorated or increased emissions; –: improved or reduced emissions).
FSN*: Filter smoke number HP*: High-pressure.

estimation of the trade-offs between EGT, efficiency, and emissions. These methodological intricacies are tailored to the objective of identifying the most promising VVA strategy for efficient aftertreatment ETM. The study not only presents demonstrated performance results but also conducts a detailed analysis of the underlying mechanisms responsible for the observed trade-offs. Consequently, an efficient and rapid warm-up of EATS by VVA will facilitate compliance with upcoming EPA Tier 5 emission legislation including a new idle NO_x standard and low-load cycle test [46]. This initiative will enhance air quality and suppress adverse environmental impacts such as global warming and rapid climate change.

2. Methodology

2.1. Experimental platform

The baseline for the research is a four-stroke, four-cylinder, off-road diesel engine. It was developed by AGCO Power for typical use in agriculture tractors and combined harvesters. Table 2 summarises the enginés technical data. The experimental work to obtain reference data shown in Fig. 4 was performed at the VTT Technical Research Centre in Finland for model calibration and validation.

Table 2
Technical data of the base engine.

Type	Off-road diesel engine
Configuration	Four-stroke, four-cylinder
Combustion mode	Conventional diesel combustion
Rated power / speed	149 kW / 1900 RPM
Max. engine load	23.8 bar (BMEP)
Boosting system	Single-stage turbocharger with electronic wastegate (Max. boost 3.5 bar. abs*)
Injection system	Common-rail direct injection with multi- pulse injection
Max. fuel injection pressure	2000 bar
Valvetrain	Fixed valvetrain by mechanical camshaft
No. of valves per cylinder	Four
IVO/IVC (at 1 mm lift)	375.6 CAD / 541.2 CAD (TDCF** 0 CAD)
EVO/EVC (at 1 mm lift)	160.9 CAD/ 345.7 CAD (TDCF** 0 CAD)
Exhaust aftertreatment system	DOC, DPF, SCR
Emission class	EU Stage-V

abs* - absolute, TDCF** - top dead centre when firing.

With a four-valve, "Mexican-hat" combustion chamber design, the enginés displacement is about five litres. Diesel fuel was distributed using a common-rail direct injection system with solenoid-type injectors, capable of multi-pulse operation. Injection and other engine control parameters are managed by a fully-open engine controller from MoTeC. The engine calibration was adapted from the original engine control unit (ECU) by running reference tests and gathering information of the actuator settings in different load points. Fuel consumption was measured by an AVL 733 s fuel scale system. The change in fuel mass was recorded over a 60-second measurement window and then fuel mass flow was calculated based on the known mass and length of the measurement window.

The engine was equipped with single-stage BorgWarner turbocharger. An electronic wastegate controlled boost pressure. The hot pressurised air from the compressor was cooled by a water-cooled charge-air cooler (CAC). A hot-film type air flow meter from ABB measured total air mass flow at the entry of air path. Various temperature and pressure readings were collected at several locations in the intake and exhaust line, as well as in the cooling and lubrication circuits for monitoring and validation. Fig. 2 is a schematic diagram of the engine test bench and instrumentation. The concentrations of gaseous components in the exhaust, such as CO, HC and NO_x, were measured with a rack of different emission measurement devices, listed with other instrumentation in Table 3. Particulate concentrations were measured with an AVL MSS analyser. All emission measurements were sampled from the raw gases taken after the turbocharger. The exhaust system did not include a lambda sensor, so the excess air ratio (λ) was calculated, based on the air mass flow and fuel flow measurement.

In-cylinder pressure profile was measured at only one selected cylinder using a piezoelectric pressure transducer (AVL GU22C) with a charge amplifier, while sensing dynamic pressure change. Zero-level correction for the cylinder pressure was performed by calculations within AVL IndiCom measurement software, using pressure difference of two points along the compression line and pre-defined polytrophic coefficient. The calculation assumes compression is adiabatic between the two points. Measurements of high-frequency pressure and engine rotational speed were triggered via an optical encoder with 0.1 CAD resolution. Engine rotational torque was sensed by an HBM T10F torque

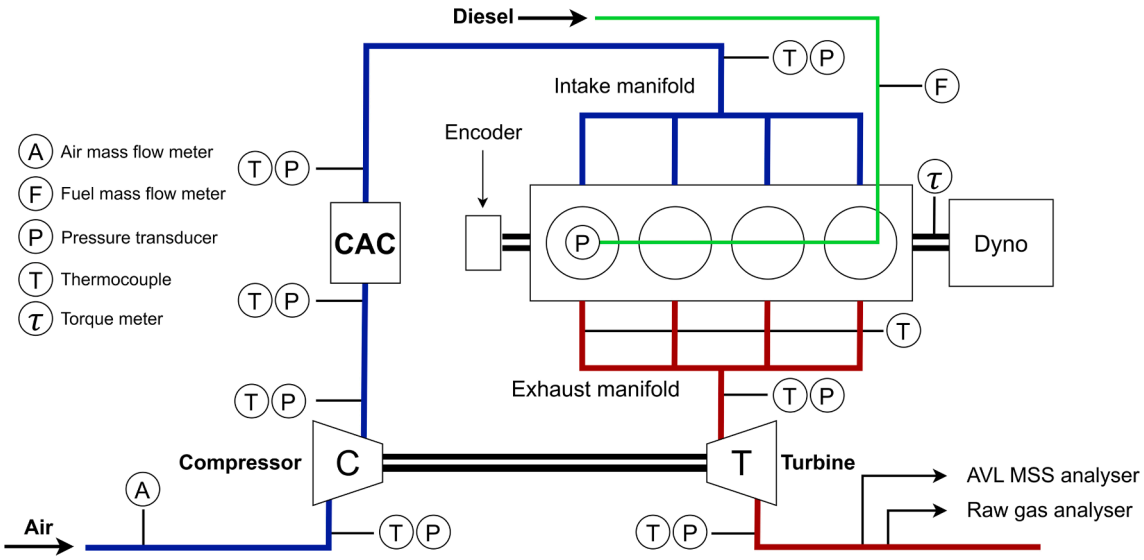

Fig. 2. Schematic diagram of engine test bench with instrumentation.

Table 3
Instrument devices and accuracy.

Type	Transducer	Measurement range	Accuracy (FS = Full Scale)
Air mass flow	ABB Sensymaster	0–4000 kg/h	0.6 % (10–100 % of meas. range)
Fuel consumption	AVL Fuel balance 733 s	0–1800 g	0.12 % of FS
Torque	HBM T10F	0-5000Nm	Accuracy class 0.1 (DIN EN ISO 376)
Pressure			
- Cylinder	AVL GU22C	0–250 bar	0.2 %
- Int./Exh. manifold	Danfoss MBS 33	0–4 bar	0.8 % of FS
- Intake pipe	Vaisala PTB100A	500–1100 mbar	0.15 mbar
- Exhaust pipe	Mûller MHDS 400 mbar	0–400 mbar (rel*)	0.1 % of FS
Temperature	K type thermocouple	0–1200 °C	1.5 °C
Exhaust composition			
- CO	Maihak AG NDIR. UNOR	1–1000 ppm	2 %
- HC	J.U.M Engineering HFID	1–100 ppm	2.5 % of FS
- NO_x	ECO Physics CLD 822	1–5000 ppm	1 %
- PM concentration	AVL MSS 483	0–50 mg/m^3	Max. 3 % at DR* of 2–10 Max. 10 % at DR* of 10–20

DR*: Dilution rate rel*: Relative.

transducer.

The engine was directly coupled with a 570 kW eddy current dynamometer (Froude AC570F) via a driveshaft with a slight horizontal offset angle. At the engine side, the driveshaft is mounted to a rubber damper to dampen the torsional vibrations. Coolant and oil temperatures were controlled by the engine's own thermostats, and so may have varied to some extent, depending on engine load and speed. The dynamometer was controlled by its own automation system, based on a programmable logic controller and in-house software. The automation system governed all thermal parameters and acquired all the low-frequency signals.

The engine was run for a pre-defined time at each operating point before taking a measurement, ensuring that the engine was thermally stabilised. All the measurements were taken during the last 60 s of a 500-second measurement stage. All the low-frequency data collection was performed with an in-house data acquisition system, consisting of modules from National Instruments. The high-frequency in-cylinder pressure trace was recorded for 100 consecutive engine cycles with an AVL IndiModul 622. The measured in-cylinder pressure data were post-processed using AVL Concerto to analyse combustion characteristics and compute general performance. A digital low-pass filter was applied to filter out combustion-induced high-frequency noise in the measured raw pressure signals. The clean pressure signals were used to compute gross and net indicated mean effective pressure (IMEP), and also the pumping mean effective pressure (PMEP), based on following equations, Eqs. (1)–(3).

$$IMEP_g = \frac{1}{V_s}\oint pdv = \frac{Area\ of\ high\ pressure\ loop}{V_s} \tag{1}$$

$$\begin{aligned} IMEP_n &= \frac{1}{V_s}\oint pdv \\ &= \frac{(Area\ of\ high\ pressure\ loop) - (Area\ of\ pumping\ loop)}{V_s} \\ &= IMEP_g - PMEP \end{aligned} \tag{2}$$

$$PMEP = \frac{1}{V_s}\oint pdv = \frac{Area\ of\ low\ pressure\ loop}{V_s} = IMEP_g - IMEP_n \tag{3}$$

where, p is instantaneous in-cylinder pressure, v is instantaneous in-cylinder volume, V_s is swept volume of a cylinder.

For combustion analysis, the gross heat release rate (HRR) and the gross cumulative heat release (CHR) were calculated, based on the first law of thermodynamics (energy balance) and a single-zone model, while considering in-cylinder heat loss ($\frac{dQ_{loss}}{d\theta}$) as follows Eqs. (4)–(7):

$$HRR = \frac{\gamma}{\gamma-1}p\frac{dV}{d\theta} + \frac{1}{\gamma-1}V\frac{dp}{d\theta} + \frac{dQ_{loss}}{d\theta} \tag{4}$$

$$\frac{dQ_{loss}}{d\theta} = A \times h_c \times (T - T_w) + \varepsilon\sigma(T^4 - T_w{}^4) \tag{5}$$

$$h_c = 130 \times v^{-0.06} \times p^{0.8} \times T^{-0.4} \times (\bar{u} + 1.4)^{0.8} \tag{6}$$

$$CHR = \int_{SOC}^{EOC} HRR d\theta \tag{7}$$

where, v is instantaneous cylinder volume, p is instantaneous cylinder

pressure, T is instantaneous cylinder bulk temperature, T_w is cylinder wall temperature, A is heat transfer area, h_c is convective heat transfer coefficient, $\overline{u}$ is mean piston speed, γ is ratio of specific heat, SOC is crank angle at start of combustion and EOC is crank angle at the end of combustion.

The change of cylinder volume (V) and pressure (p) was calculated based on 0.1 CAD. The ratio of specific heat (γ) was calculated, based on bulk cylinder temperature (T) computed by ideal gas law at each crank angle step. The heat loss model considered convective and radiation heat transfer which is significant in diesel engines. The convective heat transfer coefficient (h_c) was estimated by Hohenberg model [47] for diesel engines with swirl. The heat loss model was further corrected in the simulation process. The 5 %, 50 % and 90 % mass fraction burned (MFB) combustion phasing indicators were derived directly from the CHR curve. The model validation uses the average over 100 cycles for all cylinder pressure, temperature, IMEP, PMEP and combustion-relevant parameters.

2.2. 1D engine model set-up

A one-dimensional (1D) engine model was used to perform a model-based investigation. The research engine model was originally developed by AGCO Powerś engine performance development team, using the 1D commercial code, GT-Suite, as depicted in Fig. 3. EAT was not necessary because this studýs main aim was to investigate EGT increment accurately, along with combustion, engine-out emissions and fuel efficiency with various VVA strategies. Accordingly, EAT was not included in the engine model, although its effect on flow restriction was considered by adding an orifice component after the turbochargeŕs turbine. This is a common practice to simplify the model without losing the physical behaviour.

The virtual 1D engine model represents the entire engine system, such as intake and exhaust airpath line, turbocharger, cylinders, ECU, injectors and even cranktrain system. The turbocharger is located near the inlet and outlet boundary and was encrypted. Turbocharger performance was computed, based on its compressor and turbine performance map. Boost pressure was controlled by a boost controller with target boost level. A semi-predictive intercooler model was used for

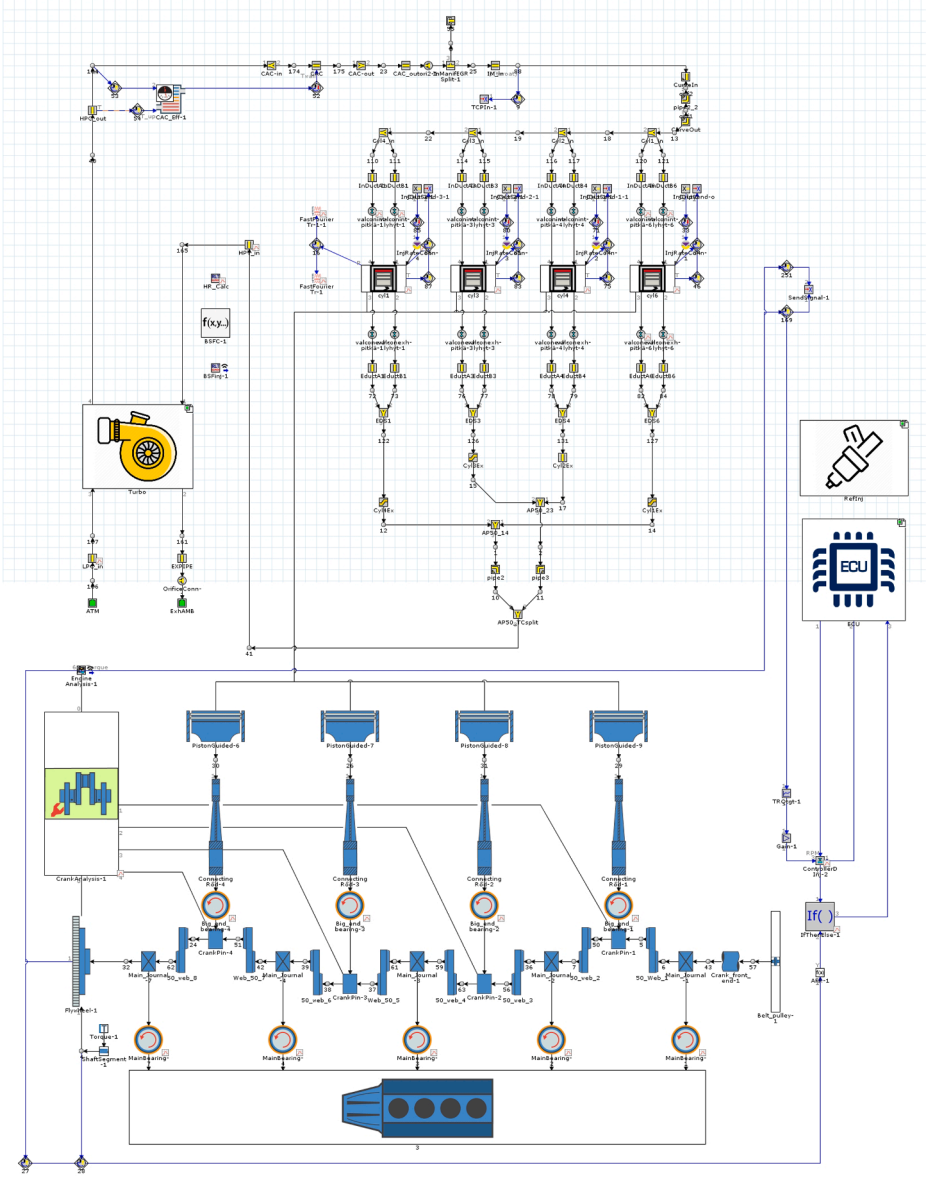

Fig. 3. 1D research engine model.

realistic cooling of compressed charges. The cranktrain system (piston, connecting rod, crankshaft, bearing, etc.) was modelled for reliable estimation of mechanical friction over different in-cylinder conditions of VVA.

The study used the predictive combustion model, DIPulse for reliable predictions of EGT, emissions and efficiency. DIPulse predicts burning rate (combustion) and associated emissions for direct-injection diesel engines with single and multi-pulse events. VVA has a direct impact on in-cylinder mixture formation and combustion, so use of the DIPulse model captures how VVA influences combustion. The model estimates burn rate profile from given injection profile and in-cylinder conditions. High-quality injection data is required to obtain an accurate combustion profile from DIPulse: this study used an extensive injection map and detailed geometry of the injectors as input data.

The DIPulse model works closely with the injector and ECU models. The ECU model has a brake mean effective pressure (BMEP) controller to maintain a constant engine load for the present study. It triggers an increase or decrease in injection rate if the current BMEP varies from the target value. Based on imposed injection profile, DIPulse estimates the burn rate profile. This feedback loop is executed until the current BMEP level is within a certain tolerance of the target BMEP.

The injector model supports multiple injection strategies, such as pilots, main and post injection. The controller adjusts only main injection quantity by varying its profile (duration) without changing injection timing and pressure. Pilot and post injection events remain constant.

A finite element solver was used to calculate heat losses in the cylinders, wall surface temperature of cylinder liner, piston, and heads, including valves and valve guides. The results were imposed on the Hohenberg model to calculate in-cylinder heat loss [47]. The Colburn heat transfer correlation was adopted for intake and exhaust pipes, while wall temperature of exhaust pipes was numerically estimated [48]. Turning to emission characteristics, an extended Zeldovich mechanism was used to model in-cylinder NO_x formation, and the Hiroyasu model was applied for soot emission [49].

2.3. Predictive combustion and emission model calibration

The predictive combustion model plays a key role in the present study to properly capture the associated effects of VVA strategies on EGT, efficiency and emissions. The baseline engine model was thoroughly parametrized and calibrated by the engineś manufacturer, AGCO Power. However, at low-load conditions that involve post injection, the baseline model calibration was not predicting the heat release and emissions within the accuracy targets. These were set at below 1 % root mean square error for the reproduced in-cylinder pressure and 5 % maximum error for NO_x emissions respectively. Relevant parameters of the DIPulse model and a reaction rate multiplier of the extended Zelodvich mechanism in the NO_x sub-model were recalibrated in order to achieve these accuracy targets.

Basically, the DIPulse model discretizes the cylinder into three thermodynamic zones: main unburned zone; spray unburned zone; and spray burned zone [50]. The modeĺs working principle is to trace fuel from injection stage to burning stage. Four sub-models are used to capture four phenomenological diesel combustion behaviours – entrainment, ignition, premixed combustion and diffusion combustion. Each behaviour is mathematically described, as shown in Eqs. (8)–(11) respectively.

$$\frac{dm_{inj}}{dt} = -C_{ENT}\ \frac{m_{inj}u_{inj}}{u^2}\ \frac{du}{dt} \tag{8}$$

$$\tau_{IGN} = C_{IGN}\ \rho^{-1.5}\ \exp\left(\frac{3500}{T_p}\right)[O_2]^{-0.5} \tag{9}$$

$$\frac{dm_{PM}}{dt} = C_{PM}\ m_{PM}\ k\ (t - t_{IGN})^2\ f([O_2]) \tag{10}$$

$$\frac{dm_{DF}}{dt} = C_{DF}\ m_{DF}\ \frac{\sqrt{k}}{\sqrt[3]{V_s}}\ f([O_2]) \tag{11}$$

where, m_{inj} is injection mass flow rate; u_{inj} is velocity at injector nozzle; u is velocity at spray tip; τ_{IGN} is ignition delay; ρ is pulse gas density; T_p is pulse gas temperature; $[O_2]$ is oxygen concentration; m_{PM} is premixed mass; k is turbulence kinetic energy; t_{IGN} is time at ignition; m_{DF} is diffusion combustion mass (remaining unmixed fuel and entrained gas mass); V_s is cylinder swept volume; C_{ENT} is entrainment rate multiplier; C_{IGN} is ignition delay multiplier; C_{PM} is premixed combustion rate multiplier; and C_{DF} is diffusion combustion rate multiplier.

Entrainment rate in Eq. (8) describes spray penetration and fuel mixing with surrounding gases when fuel is injected at each pulse. It was derived from conservation of momentum based on empirical spray penetration law [50]. The entrainment rate or air mass is inversely proportional to injection velocity (u) at spray tip. The entrainment rate is further modified by the entrainment rate multiplier (C_{ENT}). Ignition delay in Eq. (9) represents the time delay between start of injection and start of combustion, which has a significant effect on the amount of premixed charge and premixed combustion. The ignition delay is computed at each pulse, based on oxygen content ($[O_2]$), pulse temperature (T) and pulse gas density (ρ), based on the Arrhenius expression. It can be modified by the ignition delay multiplier (C_{IGN}).

Premixed combustion in Eq. (10) is the early stage of diesel combustion. This is rather rapid combustion of premixed charge accumulated during the ignition delay period. The premixed mass (m_{PM}), ignition delay ($t - t_{IGN}$) and its mixing by turbulence (k) influence the combustion directly. However, the rate of combustion is kinetically limited [50] and can be modified by a premixed combustion rate multiplier (C_{PM}). After premixed combustion, the remaining unburned fuel and entrained gas start to mix and burn in a diffusion-limited phase. This is called diffusion combustion, as described in Eq. (11). It can be reduced by engine load or long injection duration due to spray-wall and spray-spray interactions [50]. The diffusion combustion rate multiplier (C_{DF}) can adjust the combustion rate.

The four multipliers ($C_{ENT}, C_{IGN}, C_{PM}, C_{DF}$) described above need to be calibrated with experimental data in order to accurately estimate combustion behaviour. This allows adjustment to suit the intensity of each phenomenon. Calibration was performed over 10 selected operating points (OPs) with the engine manufacturerś own fixed valve settings. These calibration OPs are denoted by black markers in Fig. 4, encompassing engine speeds and load regions critical for the ETM analysis. The multipliers were fitted using GT-Suités multi-parameter optimiser.

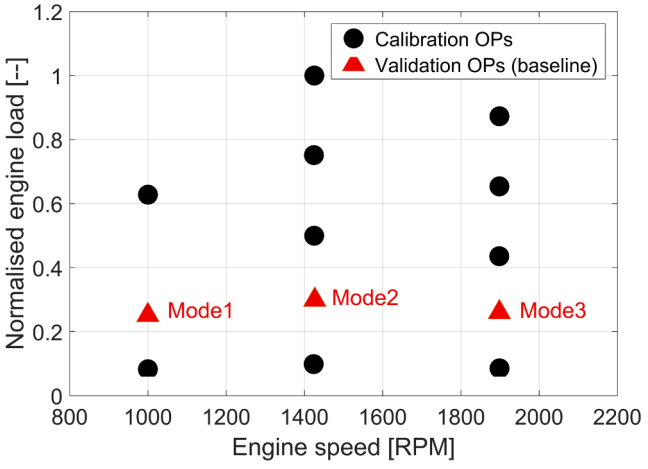

Fig. 4. Operating points for model calibration and validation.

Tuning was global level, not case-dependent. Ultimately, one set of four multipliers was obtained, valid for the entire operating envelope. Following calibration, both the predictive combustion and engine model underwent validation at three low load OPs, identified as Mode1, Mode2, and Mode3 in red in Fig. 4. The validation will be discussed further in Chapter 3.1. These three OPs, employing the fixed valve settings provided by the engine manufacturer, establish the baseline conditions for VVA simulations.

The NO_x model was calibrated with experimental data in the same manner. A NO_x calibration multiplier was tuned to adjust the net rate of NO_x formation. However, a multiplier for soot emissions was not calibrated in the present study because it is extremely challenging to predict it exactly [51]. In addition, HC and CO emissions are typically an order of magnitude lower in CI engines compared to NO_x and soot, and typically not an issue when considering EPA Tier 4 final emission limits. Thus, these sub-models were not explicitly calibrated. To this end, the model predictions of soot, HC and CO are to be treated as informative in terms of trends but not absolute values. Absolute level accuracy was validated from the NO_x emission results in this model-based study, but only for VVA cases close to the baseline valvetrain setting. For this reason, the absolute NO_x level prediction is not guaranteed for significantly early or late and unconventional valve timings.

2.4. VVA strategies and simulation conditions

VVA simulation was performed at three low-load OPs, identified as Mode1, Mode2, and Mode3 in Fig. 4. Table 4 shows simulation conditions. These three OPs, using the engine manufacturer's fixed valve settings, serve as the baseline for investigating and analysing the effect of VVA. The EATS was suffering from particularly low conversion efficiency at these points. All are below 30 % load but range from low to high engine-speeds. Based on the literature review described in the introduction, four VVA strategies were identified as interesting for diesel engine ETM. Each strategy involves two distinctive techniques of achieving the ETM target. The four strategies selected for VVA simulation are:

- Intake modulation including EIVC and LIVC
- Exhaust modulation including early exhaust valve opening (EEVO) and late exhaust valve opening (LEVO)
- Internal EGR modulation including negative valve overlap (NVO) and 2EVO
- Cylinder deactivation (CDA) and cylinder cut-out (CCO)

Three to four different valve profiles were reproduced at each technique, allowing the sensitivity of each strategy on the EGT increment to be studied. Fig. 5 shows the characteristics of each valve technique.

Fig. 5(a)–(d) illustrate valve profiles of the intake and the exhaust modulation strategies. IVC timing and EVO timing were selected as a main parameter in the intake and exhaust modulation strategy respectively, since excessive IVO and EVC modulation are constrained by low valve clearance distance due to the high compression ratio in diesel engines. For instance, advancing IVO and delaying EVC are ruled out in order to avoid collision with the piston. In addition, constant valve overlap was maintained throughout the intake and exhaust modulation, because change of valve overlap could influence in-cylinder charge mixture and thermal condition at IVC, which strongly affects EGT. This makes EGT analysis difficult since many factors are involved. For this reason, only one parameter at each technique was modulated up to 80 CAD, with an interval of 20 CAD, in both the intake and exhaust modulation.

Fig. 5(e)–(h) depict the corresponding valve profiles for the internal EGR and cylinder deactivation/cut-off strategies. In the internal EGR modulation, internal EGR fraction (or residual fraction) was changed by either NVO or 2EVO. In the NVO strategy, the high internal EGR fraction was retained by advancing EVC for early termination of the exhaust process. Although retarding IVO did not affect the amount of internal EGR, it provided promising potential to reduce pumping loss. Hence, IVO was retarded, together with advancing EVC, with an interval of 20 CAD simultaneously up to 60 CAD for better efficiency, as seen in Fig. 5 (e).

In the 2EVO strategy, the internal EGR fraction was controlled by reopening exhaust valves during the intake stroke. During the second opening, high exhaust pressure pushed burned gases into the cylinder, increasing the internal EGR effect. The period of the 2EVO was maintained while the peak valve lift was changed in three steps (2 mm, 3.5 mm and 5 mm) to vary the internal EGR fraction, as shown in Fig. 5(f). Higher peak valve lift during 2EVO enlarged the valve opening area, thus increasing the residual fraction. In fact, 2IVO was considered to be a promising strategy during the initial literature stage. However, it was not included in the final simulation study because it was identified that 2EVO outperformed 2IVO by introducing hot gases directly into the combustion process [43].

In the CDA and CCO strategy, two of the four cylinders were deactivated. Fuel injection was suspended for the deactivated cylinders. CDA also shut off both intake and exhaust valves in the deactivated cylinders, as seen in Fig. 5(g), while CCO maintained all valve operation as normal, regardless of cylinder deactivation, as seen in Fig. 5(h).

All the simulation was conducted under constant load and boost pressure conditions at each operating point as the baseline (Table 4) regardless of VVA. The simulation varied only valve timing and profile. The rest of the system remained unchanged, exactly as the baseline. Thus, any changes in behaviour are strongly attributable to VVA. Since all strategies were performed at exactly the same engine speed and torque level, this enables extensive back-to-back comparisons such as burn rate, combustion phase, gas exchange, mass transfer, emissions and fuel consumption, as well as EGT. All are comprehensively discussed in the next chapter. Note that in the present study, EGT refers to turbine outlet temperature before entering the EATS.

Table 4
Reference operating points with parameters relevant for ETM (Note that information on valve actuation and injection is further encapsulated in Fig. 5 and Fig. 7, respectively).

Simulation conditions	Mode1	Mode2	Mode3
Engine speed [rpm]	1000	1425	1900
Engine load [%]	28.8	34.3	29.8
Boost pressure ratio [–]	1.06	1.18	1.46
EGT [°C]	280	329	293

3. Results and discussion

3.1. Model validation – standard engine operation without VVA

Before investigating VVA, the calibrated model was validated over three low-load OPs (Mode1, Mode2, Mode3), as shown in Fig. 4. Fig. 6 compares the simulation results with the experimental results without VVA at these points, showing absolute and percentage error for selected key parameters. The key parameters can be divided into two groups. The first three ($IMEP_g$, P_{max} and MFB50) are good indicators to validate the predictive combustion model because they are directly influenced by the predicted in-cylinder and combustion profile. The error limits illustrated by blue dashed lines were adopted from the recommendation by GT-Suite [50]. The target limits are not that rigorous, to cover uncertainty of the predictive model over the wide operating ranges. The remaining six parameters can be used to validate the general engine performance. Their 5 % error limits are typical of those adopted in numerical engine studies to provide sufficient accuracy in representing general engine behaviours.

Overall, the DIPulse model predicted combustion behaviour well in Mode1 and Mode2. Both P_{max} and $IMEP_g$ were well within the accuracy

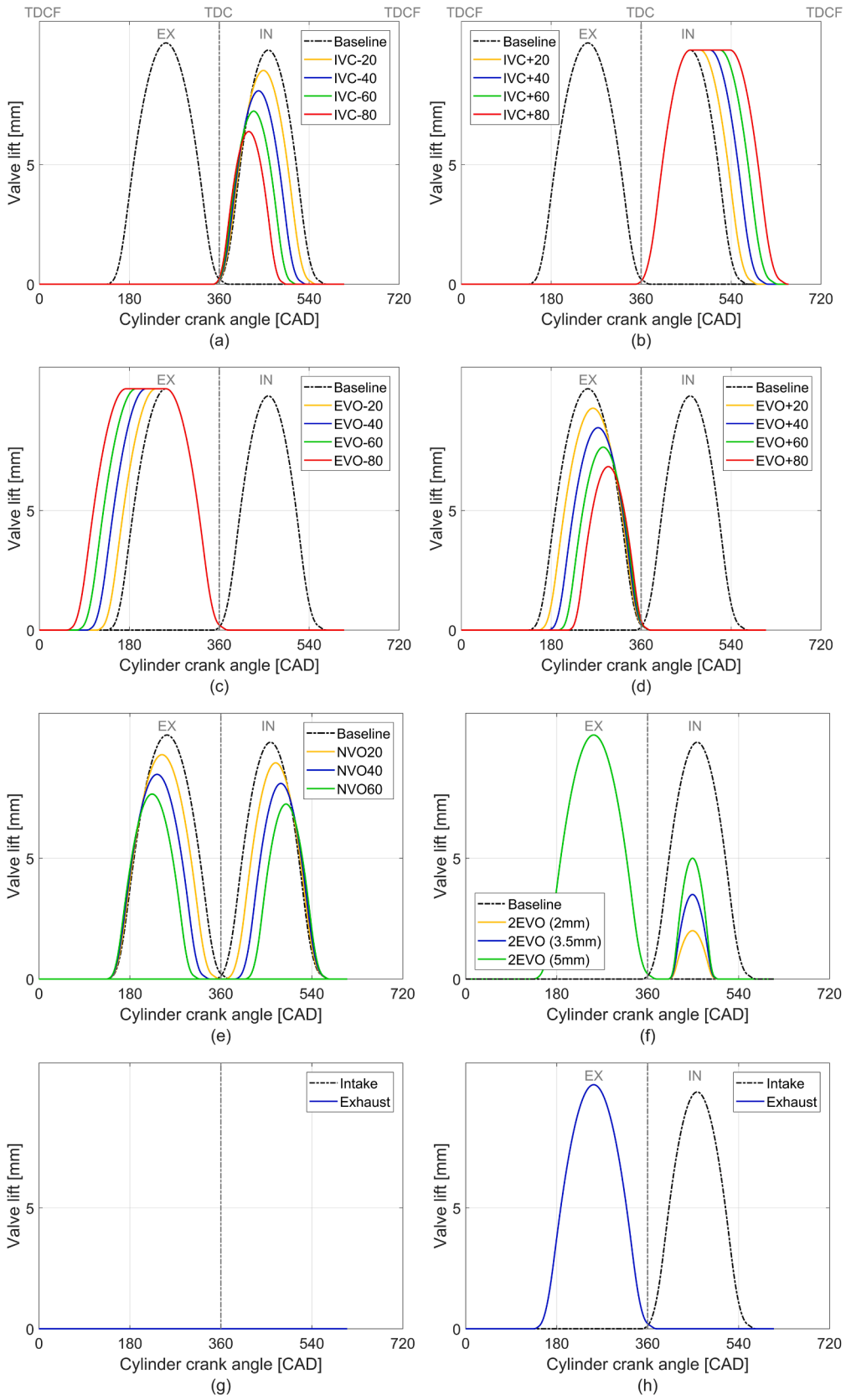

Fig. 5. The scope of simulated valve profiles: (a) EIVC; (b) LIVC; (c) EEVO; (d) LEVO; (e) NVO; (f) 2EVO; (g) CDA (deactivated cylinder); (h) CCO (all cylinders) and CDA (activated cylinders).

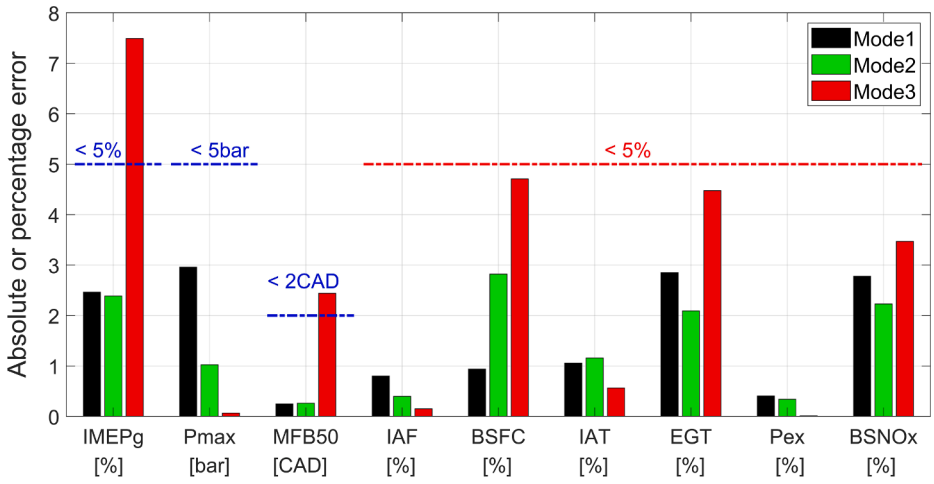

Fig. 6. Absolute or percentage errors of combustion and general engine performance parameters: gross indicated mean effective pressure ($IMEP_g$); peak in-cylinder pressure (P_{max}); crank angle of 50% fuel mass fraction burned (MFB50); intake air mass flow (IAF); brake specific fuel consumption (BSFC); intake air temperature (IAT); exhaust gas temperature at turbine outlet (EGT); exhaust pressure at turbine outlet (P_{ex}); brake specific NO_x ($BSNO_x$) at Mode1, Mode2 and Mode3.

target of 5 % and 5 bar. In addition, the error of MFB50 did not exceed 0.5 CAD. But the model's predictions were less accurate in the mentioned parameters in Mode3. Here, although the P_{max} was well-captured, the $IMEP_g$ was underpredicted, with 8 % error compared to the measurement results. This correlated with a large error (2.5 CAD) in estimating MFB50.

Fig. 7 compares simulation and experimental results for in-cylinder pressure and gross heat release rate (HRR) at Mode3. They help explain the discrepancies in the $IMEP_g$ and MFB50 results. It is apparent that the model predicts the profile of HRR very well until approximately 30 CAD after TDC. The simulation's inaccuracy evidently stems from the under-predicted HRR from the late post injection (SOI4). The model predicts here a distinctively pre-mixed combustion, while the experimental HRR shows an elongated afterburning phase. Furthermore, the total amount of heat released in this phase is underpredicted by the model, which results in lower simulated in-cylinder pressure during expansion. This explains the earlier noted discrepancy in $IMEP_g$ for Mode3 (Fig. 6).

There are two possible reasons for the model's inaccuracy around late post-injection prediction. The first pertains to the accuracy of model input. The DIPulse model uses injector mass-flow rate to calculate HRR. This input cannot be directly measured during engine operation and instead is obtained from injector characterisation, assuming mean-value rail pressure during all injection events. However, in real engine operation the common-rail pressure drops momentarily after the main post-injection, causing reduced fuel rates and slower, more mixing-controlled combustion for the following post-injection dose. Secondly, while this inadequacy of the input data could be mitigated by model tuning, large post injection is seldomly represented in the calibration data. It is noted that other validation points – Mode1 and Mode2 - also incorporate post injections, but the order of magnitude of these is lower than in Mode3.

In other words, the model's predictivity at Mode3 is far outside its calibration matrix, forming the most challenging case for simulation. Bearing this in mind, the model results are considered acceptable, especially as the combustion reproduction inaccuracies diminish when considering engine-level parameters relevant to the present study. This is clearly seen in the BSFC and exhaust thermal state parameters in Fig. 6. The model's inaccuracy in Mode3 is obviously larger than in other validation cases, but well in line with the 5 % target for EGT and BSFC. The same applies to NO_x emissions ($BSNO_x$), which were predicted with relative error below 3.5 % in all cases.

In conclusion, the model is predictive in terms of VVA's effects on combustion, and its accuracy in terms of thermal state, performance and emission parameters substantiates its use for the current research. Nevertheless, in extreme valve timings, the model predictions should be regarded as indicative in terms of trends rather than absolute values, especially where combustion-related effects are considered.

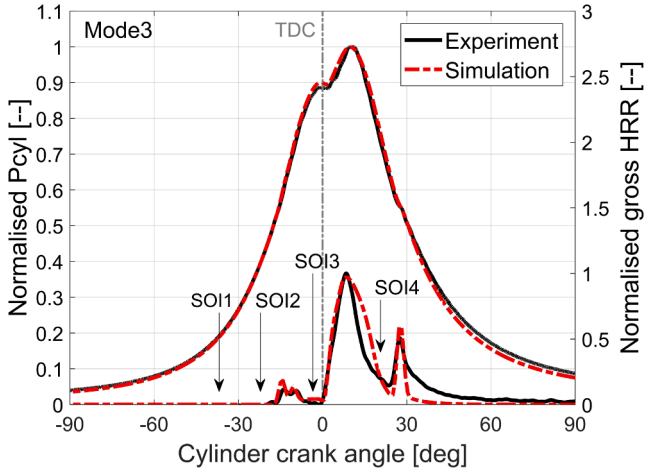

Fig. 7. Comparison of normalised cylinder pressure (P_{cyl}) and normalised gross heat release rate (HRR) at Mode3 (the least accurate).

3.2. *Effect of intake modulation (EIVC and LIVC)*

Fig. 8 presents the results of simulating EIVC and LIVC, showing changes to the governing engine parameters with respect to the baseline at the validated points of Mode1-3. It is evident that one can elevate EGT by as much as +150 °C by both advancing and retarding the IVC timing by the theoretically allowable interval. The increase in the EGT is due primarily to reducing the intake air flow (IAF), as shown in Fig. 8(b). Intake flow reduction potential, and hence the EGT increment, are stronger with EIVC and are a direct result of shortened intake duration and reduced valve lift (see Fig. 5a for reference). LIVC's effect on IAF and ΔEGT is qualitatively the same as for EIVC, but is due to different phenomenology. Note that here the maximum valve lift is unchanged (Fig. 5b) and the restriction of intake flow comes from increased backflow to the intake manifold when intake valves are still open during the compression.

In both cases, the reduced IAF influence in-cylinder heat capacity. Fig. 9 illustrates in-cylinder heat capacity of excess air at Mode2, showing that intake modulation reduces in-cylinder heat capacity

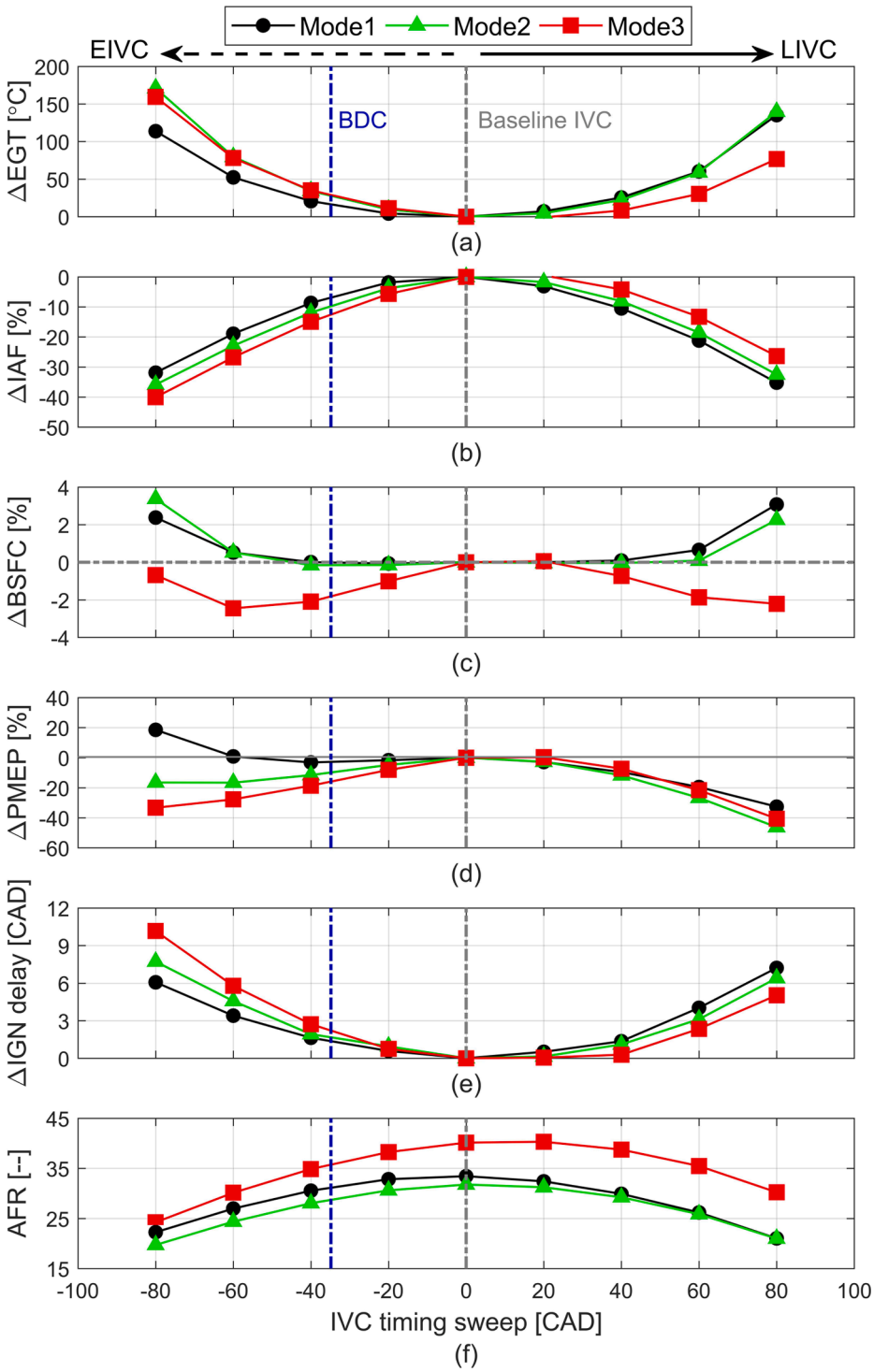

Fig. 8. Simulation results of EIVC and LIVC: (a) ΔEGT; (b) ΔIAF; (c) ΔBSFC; (d) ΔPMEP; (e) Δignition delay; and (f) in-cylinder air–fuel ratio (AFR).

compared to the baseline. The reduction of mass flow by EIVC/LIVC incurred low heat capacity, resulting in less heat being absorbed during combustion. Consequently, the lower heat capacity elevates cylinder temperature, increasing the EGT (Fig. 8a).

Fig. 10(a) shows combustion temperature in the burned zone for EIVC and LIVC at Mode2. With retarded IVC timing, the burned zone temperature beyond 30 CAD after TDC increased due to the low heat capacity effect. Thus, when the exhaust valve opened, hotter combustion gases were discharged, raising the EGT. Even though EIVC and LIVC appear to have similar combustion temperatures in the figure, EIVĆs actually is slightly higher where EIVC had slightly more reduction in air flow than LIVC at the same degree of IVC shifting, as seen in Fig. 8(b). This reduced the heat capacity (Fig. 9) and then raised EGT. It is apparent that in-cylinder heat capacity is a main parameter to control in-cylinder thermal status and EGT when using EIVC and LIVC.

Both EIVC and LIVC had greatest effect on EGT at their most extreme IVC timings. The EGT increment is +171 °C (IVC-80) and +140 °C (IVC+80) respectively at Mode2, corresponding with 36 % (IVC-80) and 33 % (IVC+80) of flow reduction. EIVC produced +31 °C higher EGT than LIVC because its flow restriction was three percentage points

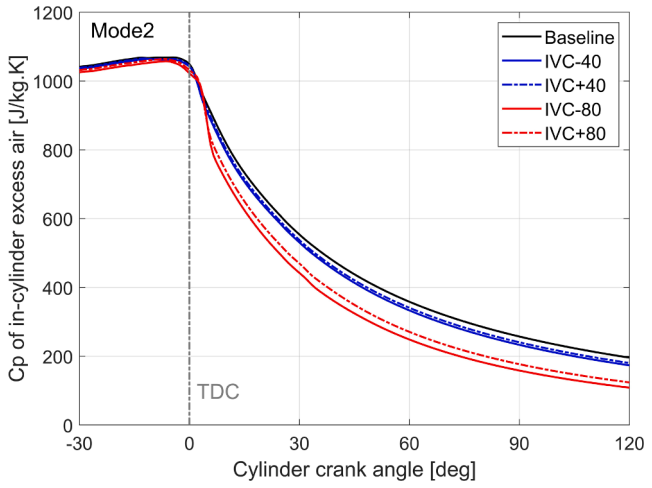

Fig. 9. Trace of specific heat capacity (c_p) of excess air at Mode2 during combustion.

greater, lowering in-cylinder heat capacity. LIVC performed better at Mode1, while EIVC was better at Mode3. These results reflect the maximum reduction of air mass flow at each operating point. Therefore, the effect of EIVC and LIVC on EGT is dependent on the reduction of total air mass flow, which determines in-cylinder heat capacity.

Fig. 8(c) shows an inconsistent BSFC trend. BSFC in Mode1 and 2 was similar to the baseline up to ±60 CAD but then increased by more than 2 % at IVC-80 and IVC+80. However, fuel consumption in Mode3 was 2 % lower than the baseline. In general, BSFC is closely related to pumping work, but in this study the BSFC trend does not match the PMEP trend, depicted in Fig. 8(d). PMEP was reduced in most cases of intake modulation. The similar trend was observed in literature [52,53]. It is noted that lower trapped mass with EIVC and LIVC attributes to reduced resistance during compression, leading to a decrease in pumping losses. Thomas [53] highlighted that a higher degree of IVC modulation provides higher PMEP reduction potential. However, reduction of PMEP does not contribute to decreasing BSFC in the present study, except in Mode3. This indicates that there must be another factor, other than pumping losses, influencing BSFC. For this reason, combustion behaviour was examined.

In fact, EIVC and LIVC exert a strong impact on combustion. Shifting IVC timing reduced effective compression ratio so that cylinder pressure and temperature were lower than the baseline at the end of compression stage. Fig. 11 shows the bulk in-cylinder temperature during compression stroke at Mode2 for different LIVC cases. Cylinder temperatures at the point of pilot and main injections with IVC+80 were 60 to 70 °C lower than the baseline. Consequently, peak cylinder pressure and peak cylinder temperature gradually reduced with shifting IVC timing, as observed in Fig. 10(a) and (b). The same trend was observed with EIVC. Low cylinder temperature with EIVC and LIVC means the air–fuel mixture takes longer to reach self-ignition temperature, increasing the ignition delay time. Larger shifts in IVC timing lead to even lower cylinder temperatures and hence greater ignition delays. Fig. 8(e) shows ignition delay was prolonged by up to 10 CAD at IVC-80 and IVC+80. This delay helped to enhance premixed combustion, as shown in Fig. 12, because the additional air–fuel mixing time increased the amount of premixed mixture.

Ultimately, the long ignition delays as shown in Fig. 8(e) shifted the whole combustion process. This is most noticeable at extreme IVC timings, IVC−80 and IVC+80, where longer ignition delay slowed combustion (long combustion duration) and delayed MFB50. This indicated that more fuel is burned when the piston is moving downward, not near TDC. This caused less effective work transfer and so increased BSFC. Therefore, BSFC was affected by the combined effects of PMEP and combustion.

Mode1 and 2 show stable BSFC with moderate shifts of IVC timing up to ±60 CAD, where reduction of PMEP is offset by delayed combustion. However, it seems that the reduction of PMEP is stronger than the delayed combustion, so BSFC was reduced at Mode3. At the most

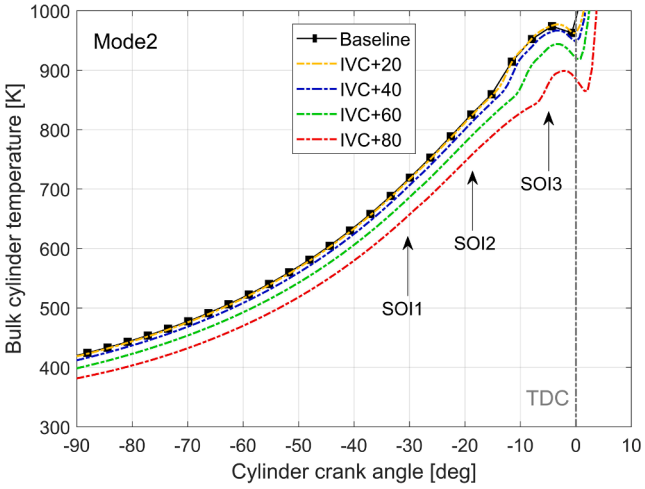

Fig. 11. Simulation results of LIVC at Mode2: bulk cylinder temperature.

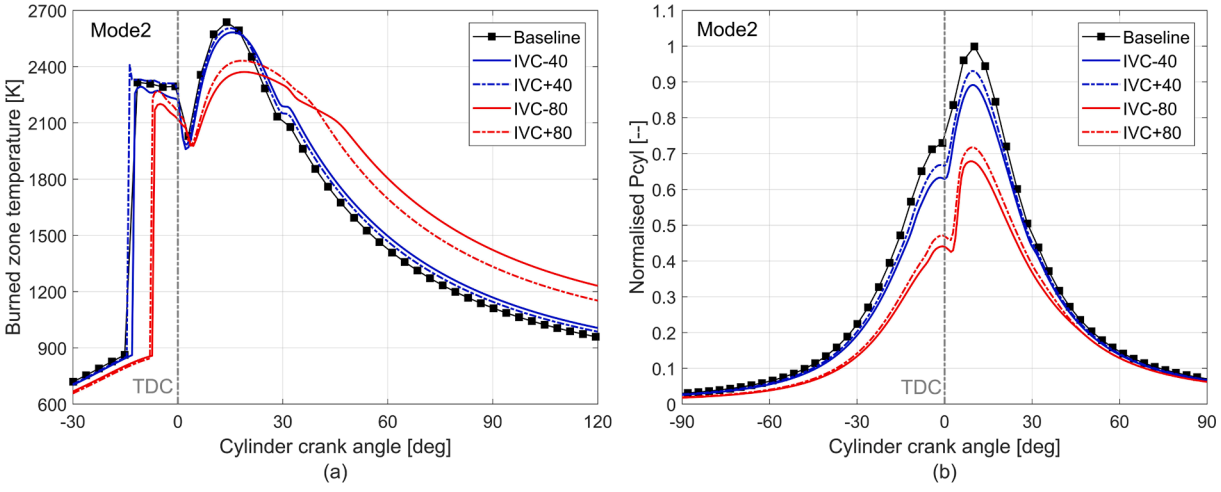

Fig. 10. Simulation results of EIVC and LIVC at Mode2: (a) burned zone temperature and (b) normalised in-cylinder pressure (P_{cyl}).

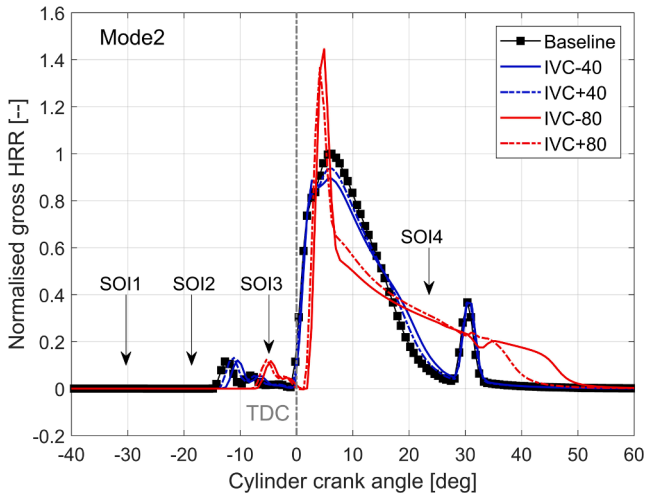

Fig. 12. Simulation results of EIVC and LIVC at Mode2: normalised gross HRR.

extreme IVC conditions (IVC−80 and IVC+80), BSFC increased sharply because combustion is slowed too much by excessive phase delay, so milder intake modulation is suggested in order to avoid increasing fuel consumption. Another measure entails advancing the combustion phase to mitigate the delay. Two methods are available for advancing the combustion phase: adjusting injection timing and internal or external EGR. De Ojeda [42] demonstrated maintenance of combustion phase (MBF50) by advancing injection timing with EIVC, improving BSFC by 4.5 % and raise EGT about 95 °C. Guan et al. [41] employed internal EGR with LIVC to reduce ignition delay by introducing hot residual gases. This resulted in reducing the BSFC penalty by 0.7 % while increasing EGT by 62 °C.

Fig. 13 shows how the change of combustion characteristics influenced engine-out emissions. LIVC and EIVC reduced peak combustion temperature due to low effective compression ratio and delayed combustion phase, as shown in Fig. 10(a). The lower peak combustion temperature gradually reduced NO_x emissions (Miller effect), as seen in Fig. 13(a). The maximum NO_x reduction of more than 97 % was observed at IVC+80 and IVC-80. Some points are even below EU Stage-V NO_x limit (0.4 g/kWh). However, Fig. 13(b) shows that extreme IVC modulations drastically increased soot emission because the air mass flow was substantially decreased. This enriched the fuel mixture, as shown in Fig. 8(f), promoting soot formation. Furthermore, the reduction in excess air constrained soot oxidation, despite increased combustion temperature.

Fig. 13(a) and (b) depict a typical diesel engine trade-off between soot and NO_x up to ±60 CAD. However, this trade-off disappears at IVC−80 and IVC+80, where both NO_x and soot were mitigated simultaneously. This is typical when combustion moves from mixed-control to premixed mode and can be clearly seen from Fig. 12's HRR plot. Towards particularly early/late valve timings, elongated ignition delay enables more time for fuel to premix, and increased local oxidizer availability

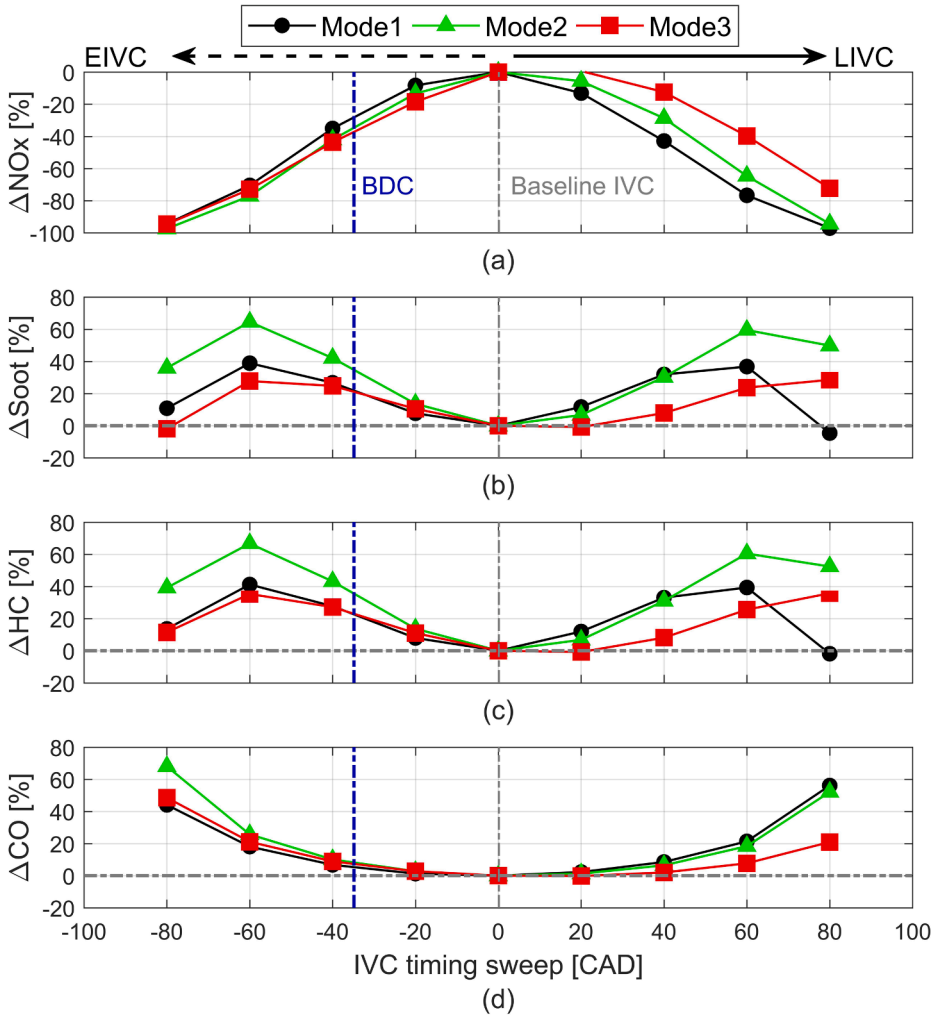

Fig. 13. Simulation results of engine-out emissions from EIVC and LIVC: (a) ΔNO_x; (b) ΔSoot; (c) ΔHC; and (d) ΔCO.

suppresses soot formation. Note however, that the results of the predictions of the combustion/emission sub-model at extreme valve timings have not been validated, and so should be treated with caution.

Fig. 13(c) and (d) show that modulating IVC timing increased HC and CO emissions. These emissions are unburned and partially burned fuels, representing incomplete combustion. Both EIVC and LIVC reduced the fresh charge flow and trapped air mass, so there was insufficient oxygen for the injected fuel. Even though increased ignition delay gave more mixing time, locally rich mixture resulted in incomplete combustion. Guan et al. [41] and Garcia et al. [55] highlighted that low combustion temperature also contributed to incomplete combustion, thereby increasing HC and CO emissions. Moreover, the oxidation process of HC and CO in the combustion chamber is suppressed by the reduced excess air. Nevertheless, the DOC's improved conversion efficiency due to elevated EGT will effectively mitigate HC and CO, leading to low tailpipe HC and CO emissions.

In short, intake modulation could elevate EGT more than 150 °C by controlling in-cylinder thermal status with air flow. Extreme IVC modulation raises EGT significantly, but produces considerable changes in combustion characteristics, such as long ignition delay, so entails a minor fuel penalty due to delayed combustion. The fuel penalty can be minimised by adjusting fuel injection timing or introducing EGR. Intake modulation also gave significant reductions of NO_x via the Miller effect, but soot, HC and CO emissions deteriorated due to the rich mixture. Increasing the air–fuel ratio can reduce these emissions but will also reduce the EGT increment.

3.3. *Effect of exhaust modulation (EEVO and LEVO)*

Fig. 14 plots simulation results of exhaust modulation. Fig. 14(a) shows an increasing EGT trend as EVO timings move further away from the baseline. Both extreme EEVO and LEVO achieved the highest EGT increments. EVO−80 raised EGT by +101 °C; EVO+80 raised EGT by +68 °C. But these excessive EVO timings also carried significant BSFC penalties of +16.6 % (EVO−80) and +13.3 % (EVO+80), as seen in Fig. 14(c). Compared to intake modulation, the EGT increment is rather

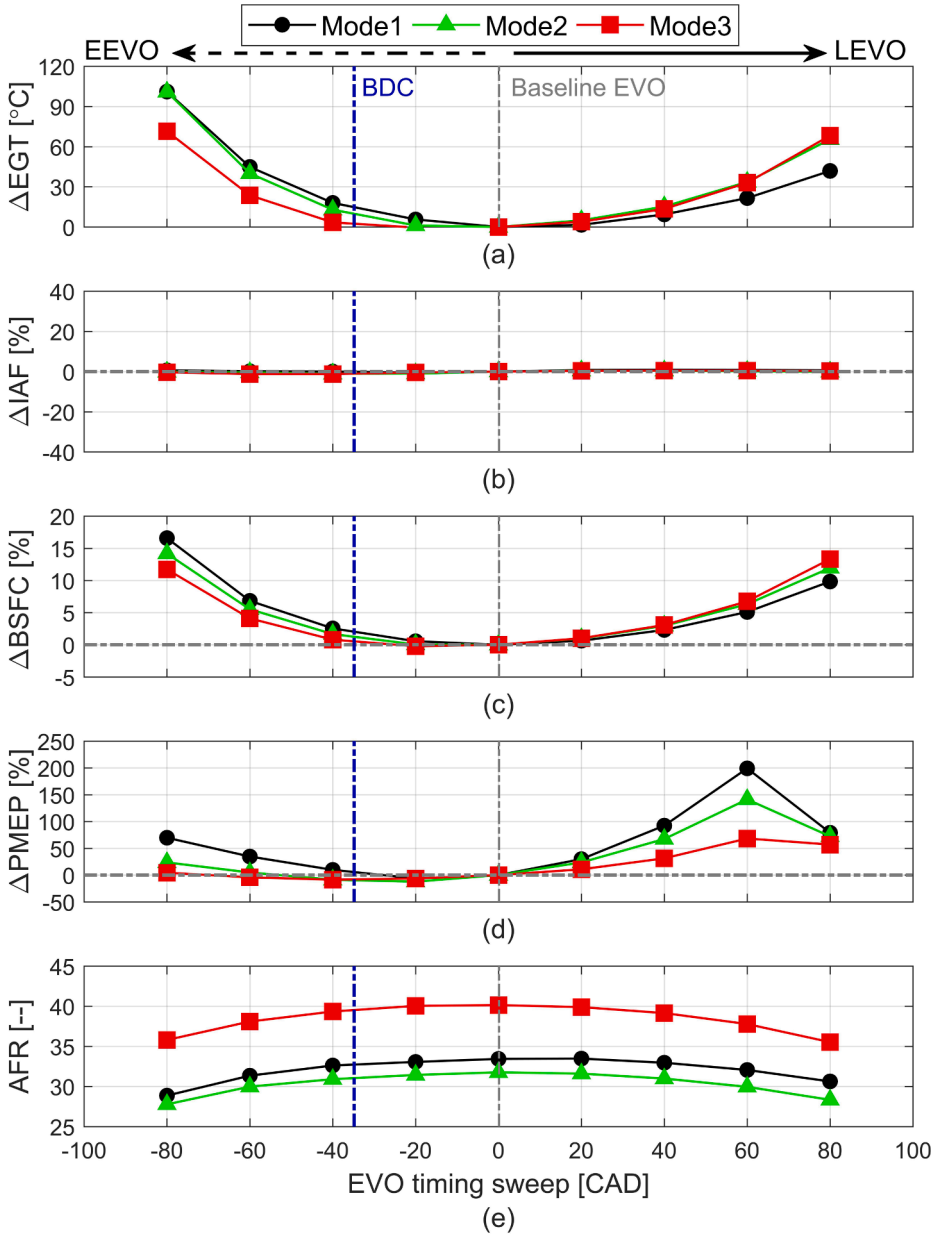

Fig. 14. Simulation results of EEVO and LEVO: (a) ΔEGT; (b) ΔIAF; (c) ΔBSFC; (d) ΔPMEP; and (e) AFR.

low and the BSFC penalty is high. Unlike intake modulation, the EGT increment is not related to air flow, since air flow (IAF) remains constant, as shown in Fig. 14(b). Constant boost pressure and unchanged intake valve profile gave constant intake flow.

Instead, exhaust modulation's ability to raise EGT is associated with how EVO timing affects the point at which combustion ends. In the power stroke, EVO timing determines when combustion will be halted. Advancing EVO timing discharges more hotter combustion gases because combustion ceases earlier. This moves the temperature at EVO towards peak temperature regions, as shown in Fig. 15(a). The high in-cylinder thermal status was achieved by reduced expansion work (prevent temperature drop) and short residual time (less heat losses). However, advancing EVO timing gradually reduced the gross work because combustion was terminated earlier. This degraded both torque and power. To maintain the same engine performance, fuel injection needs to be increased to compensate performance drop, causing a high BSFC penalty with EEVO.

Delaying EVO timing postpones the end of combustion even after bottom dead centre (BDC). After BDC, piston is moving upward but exhaust valves are still closed, so the in-cylinder charge is compressed. In our case, cylinder pressure rose to 3 bar where usually exhaust pressure is below 2 bar at low load, even though it depends on turbocharger operation. This promoted the high cylinder temperature seen in Fig. 15(b) and thus higher EGT. The later the EVO timing, the higher the EGT, due to re-compression. However, the re-compression induced high pumping work during the gas exchange process. Once again, more fuel injection is inevitable to maintain the same performance, resulting in a high BSFC penalty, even though expansion work is maximised in LEVO cases.

EEVO demonstrated better EGT performance than LEVO for the same degree of EVO modulation. The main reason is that EEVO directly released hot gases, while LEVO was involved with long expansion and re-compression which increased heat losses. Both exhaust modulations caused rather high BSFC penalties of up to +13.3 % (EVO+80) and +16.6 % (EVO−80). The BSFC increment stems from pumping work (LEVO and EEVO) and reduction of gross work (EEVO). It is noted that EVO modulation strongly affects the gas exchange process and power cycle. However, neither EEVO nor LEVO has a major effect on combustion behaviour because intake flow and in-cylinder charge condition (at IVC) before the combustion remained similar to the baseline. As a result, combustion and the cylinder pressure profiles were fairly consistent for all cases. This combustion stability makes implementation of exhaust modulation easier because combustion recalibration is not needed.

Fig. 16 provides engine-out emissions for all EEVO and LEVO cases. Variation of NO_x emission was rather small (less than 20 %) because combustion was not influenced by EVO modulation. This is related to the relatively stable peak combustion temperatures, seen in Fig. 15(a), compared to other strategies (see Fig. 10a for reference). Fig. 16(b) and (c) shows greater EVO modulation increased both soot and HC. Soot formation was promoted by rich mixture with changing EVO, as seen in Fig. 14(e). Unlike intake modulation, the rich mixture was created by increased fuel injection. Overall, EEVO indicated slightly higher soot than LEVO. This is because EEVO had less residual time, which interrupted the oxidation process.

EEVO also showed higher HC than LEVO. The reduced combustion duration with EEVO curtailed complete combustion, which increased HC. This effect was strongest at most advanced EVO case (EVO−80) where post-injected fuel had less time to be burned: LEVO gave longer combustion time, enabling a more complete burn. LEVÓs longer combustion also gave more oxidation time. This combination of long combustion and oxidation time contributed to slightly lower HC with LEVO. Fig. 16(d)́s CO emission trend is noticeably different from the others. Two factors caused LEVÓs high CO emissions. One is increased incomplete combustion of the rich mixture; the other is increased partial oxidation of HC from the long oxidation process. In contrast, CO with EEVO was lower than the baseline. This is probably attributable to reduced combustion efficiency. Note that CO has very low activation energy and so is generally easier to oxidise than HC. CO emission is preliminary attributed to local oxygen deficiencies, so less HC undergoing combustion leaves more oxygen surplus for complete oxidation of CO.

Exhaust modulation increased EGT by up to +100 °C, but with a high BSFC penalty of more than +10 %. EGT increment is controlled by changing combustion duration, but it has negative effect on fuel efficiency due to loss of expansion work (EEVO) and high pumping work (EEVO and LEVO). Furthermore, different combustion duration produced different emission trends. Despite changing combustion duration, combustion characteristics were not influenced, so NO_x emissions were not heavily affected by EVO modulation. Lastly, excessive EVO modulation should be avoided because it carries a high fuel penalty.

3.4. *Effect of internal EGR (NVO and re-introduction of exhaust)*

Fig. 17 presents the simulation results of i-EGR. First, increasing NVO and increasing valve lift of 2EVO both promoted more dilution effect. This is indicated by residual gas fraction (RGF) in Fig. 17(a). Fig. 17(b) shows that both NVO and 2EVO elevated EGT and that the increase is proportional to the EGR effect. The EGT increment was +205 °C (NVO60) and +120 °C (2EVO with 5 mm lift) respectively. The EGT

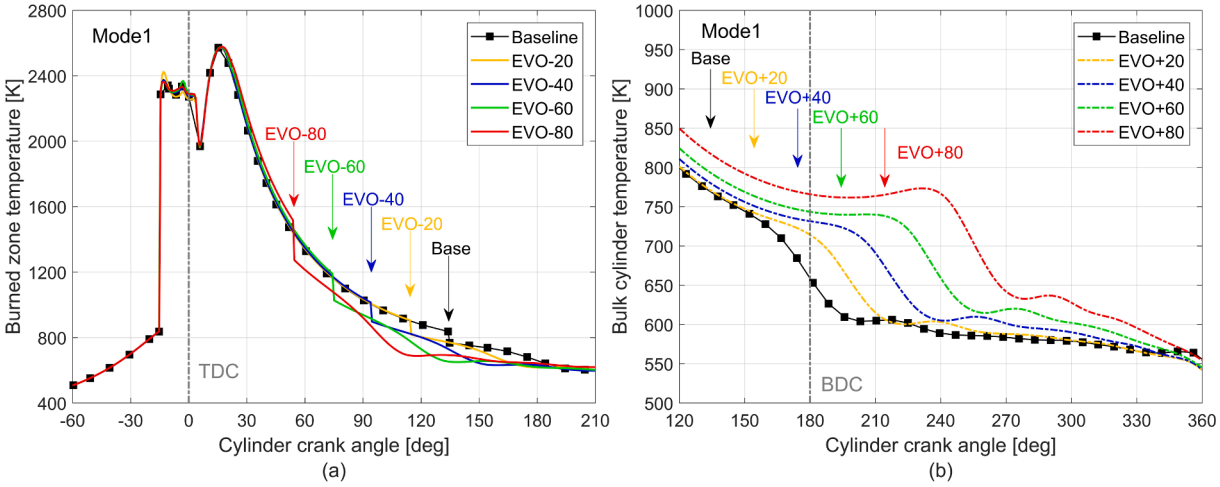

Fig. 15. Simulation results at Mode1: (a) burned zone temperature in EEVO; and (b) bulk cylinder temperature in LEVO.

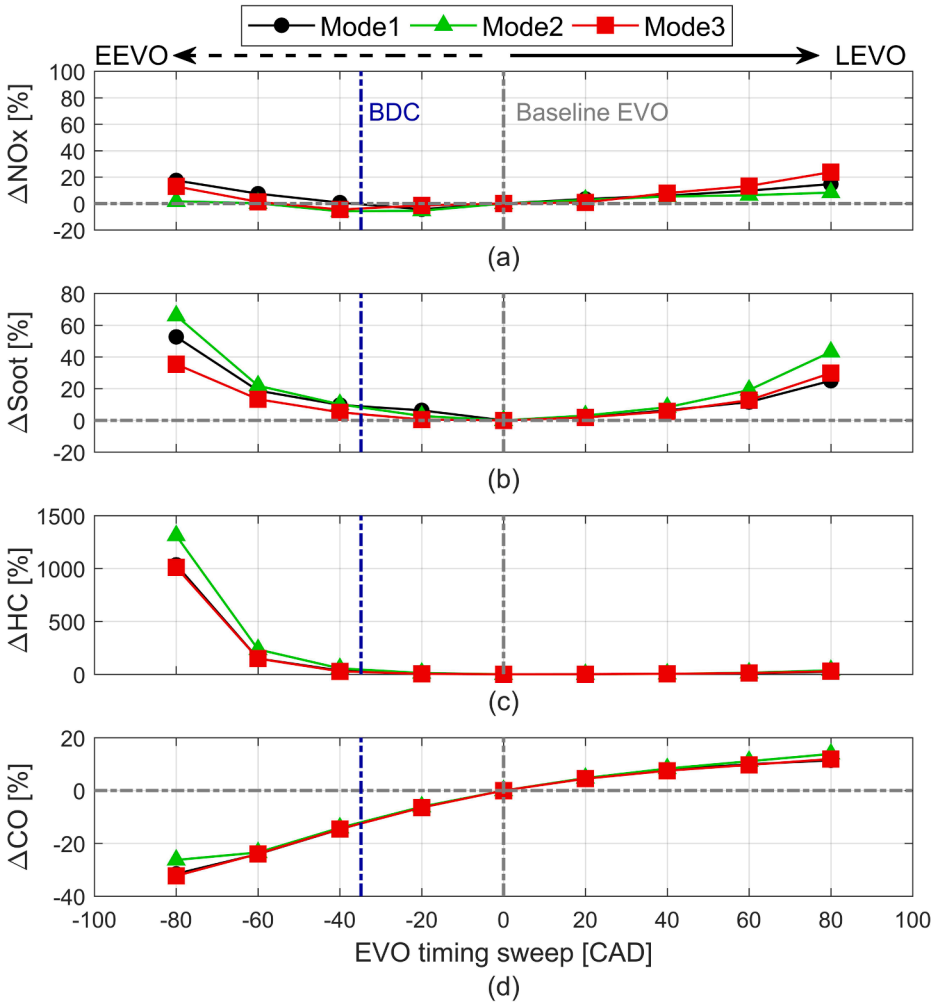

Fig. 16. Simulation results of engine-out emissions from EEVO and LEVO: (a) ΔNO_x; (b) ΔSoot; (c) ΔHC; and (d) ΔCO.

increment mechanism is rather similar to intake modulation. A higher i-EGR suppressed fresh charge induction, which reduced in-cylinder heat capacity, as seen in Fig. 17(c). This raised combustion temperature and then EGT. Fig. 18(a) displays increasing combustion temperature due to the effect of low heat capacity with increasing dilution effect in NVO and 2EVO at Mode2.

However, the reduction mechanism of air flow is different. Intake modulation directly restricted intake flow by shifting IVC timing. On the other hand, i-EGR utilised RGF to constrain intake flow. Increasing the NVO period by advancing EVC trapped more RGF because the exhaust cycle was halted earlier. High RGF in the cylinder prevents induction of fresh charges in the next cycle, cutting incoming air mass flow.

2EVO allowed backflow during intake stroke because exhaust pressure is usually higher than intake pressure at low-load operation. Increasing the maximum valve lift increased effective valve opening area, thus raising RGF. However, air flow reduction occurred at the same cycle, as shown in Fig. 18(b), which illustrates instantaneous mass flow via intake and exhaust valves. With both intake and exhaust valves open, the higher degree of backflow (high RGF) countered the incoming flow, creating resistance for the incoming charge. Fig. 18(b) clearly shows the backflow's suppression of the incoming charge.

Fig. 17(b) and (c) show that increasing RGF with either NVO and 2EVO restricted incoming charge flow, which improved EGT. Although direct comparison of NVO and 2EVO is difficult, NVO produced the higher EGT. This is mainly because NVO achieved more EGR in the current study. NVO60 raised RGF to 29 %, which cut intake air flow by 40 %. 2EVO with 5 mm valve lift raised RGF to 24 %, reducing air flow by 31 %. Thus, NVO60 showed greater EGT increment. However, the RGF of NVO20 was lower than 2EVO with 2 mm lift, so 2EVO raised EGT further. It is evident that RGF is the main parameter to control EGT in i-EGR. Results with 2EVO in particular reveal the strong relationship between RGF and EGT. In 2EVO, RGF increment is more noticeable at 2 mm lift, so the EGT increment also is large. But with higher lifts, the incremental RGF diminishes when compared with the NVO cases, so the increase in EGT also begins to flatten.

Although a large amount of EGR is effective in raising EGT, it harms fuel efficiency. Both NVO and 2EVO exhibit an increasing BSFC trend in Fig. 17(d). NVO's BSFC penalty was up to +15.7 % (NVO60), while 2EVO's was less severe, at up to +6.5 % (5 mm lift). NVO's higher BSFC penalty resulted from increased pumping work, as shown in Fig. 17(e). This is mainly due to re-compression by EEVC and re-expansion by LIVO during NVO, which is clearly visible in Fig. 19. Cylinder pressure was raised by more than 10 bar during the gas exchange process, which has a negative effect. This behaviour became more severe with a long NVO period at Mode1 and 2. However, PMEP was reduced at Mode3. In fact, the baseline pumping loop is rather large due to substantial pressure gradient between intake and exhaust. NVO reduced Mode3 pumping losses by narrowing the pumping loop via re-compression and re-expansion. Nevertheless, PMEP is not the main cause of increased BSFC, because 2EVO and NVO (Mode3) still carry a BSFC penalty, despite their pumping work being lower than the baseline. Further analysis of the combustion behaviour was required to investigate the BSFC penalty in i-EGR.

Fig. 20 presents the predictive combustion model's HRR at Mode2.

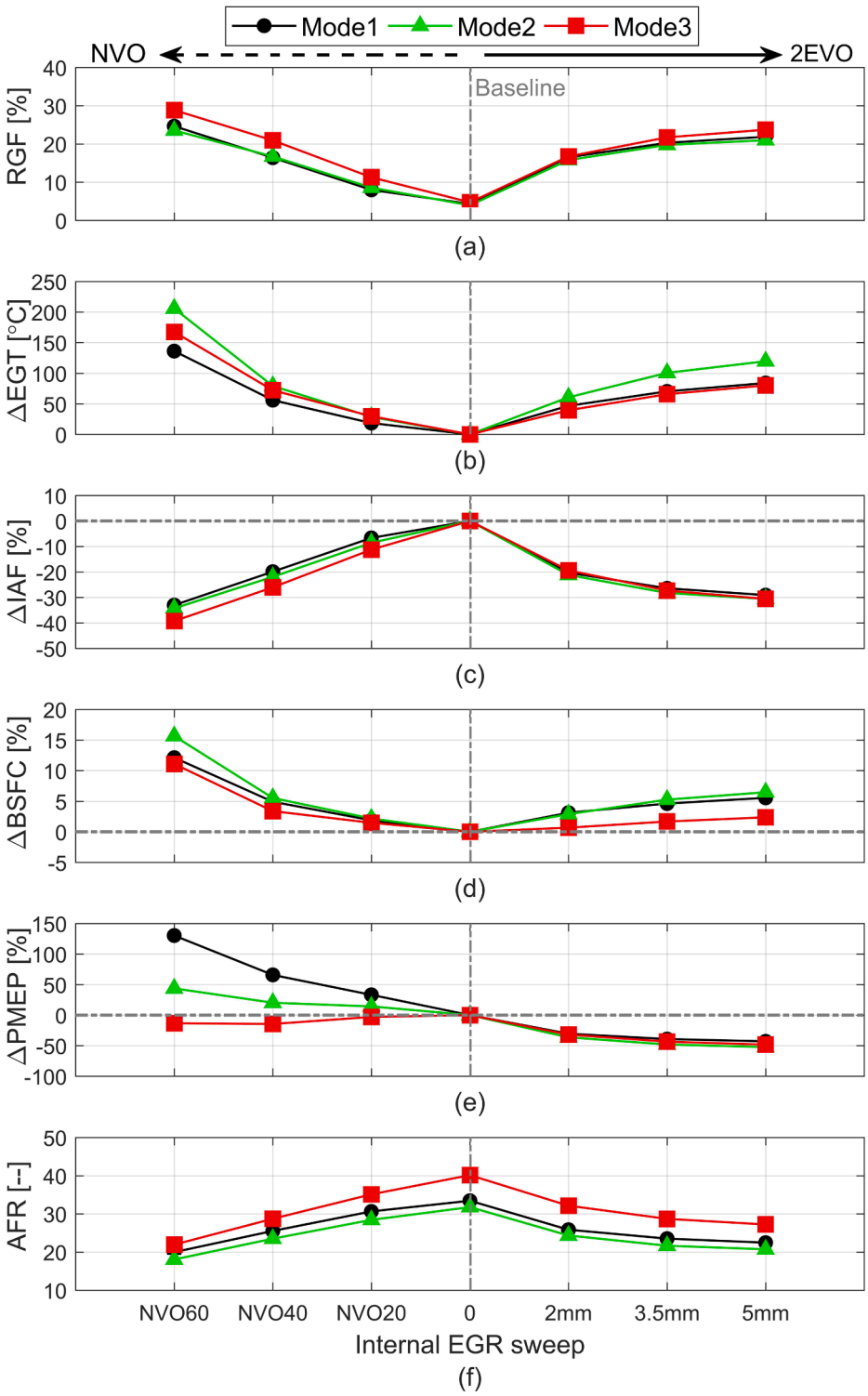

Fig. 17. Simulation results of NVO and 2EVO: (a) RGF; (b) ΔEGT; (c) ΔIAF; (d) ΔBSFC; (e) ΔPMEP; and (f) AFR.

Both NVO and 2EVO show reduced premixed combustion behaviour with increasing EGR rate, which is opposite to intake modulation. This behaviour was observed at other operating points. Since less fuel is burned at the early stage of the combustion, more fuel is burned at the later stage, which is diffusion combustion mode. Therefore, combustion duration was prolonged with increasing EGR fraction. It is widely known that EGR slows down combustion due to reduced oxygen content, which corresponds to our results. This phenomenon is clearly visible in Fig. 20. NVO60s combustion duration in particular is much longer than that of 2EVO with 5 mm lift, reflecting the higher EGR effect of NVO60 in Mode2.

Ultimately, the slow and delayed combustion caused ineffective work transfer and reduced performance because more fuel was burned far from the sweet spot near TDC, and more slowly. Injection of more fuel is essential to maintain the same performance, contributing to deteriorating fuel efficiency in both cases. Fig. 20 shows that NVO60 in particular underwent more changes in combustion phase and duration than 2EVO with 5 mm lift, and thus recorded a larger fuel penalty.

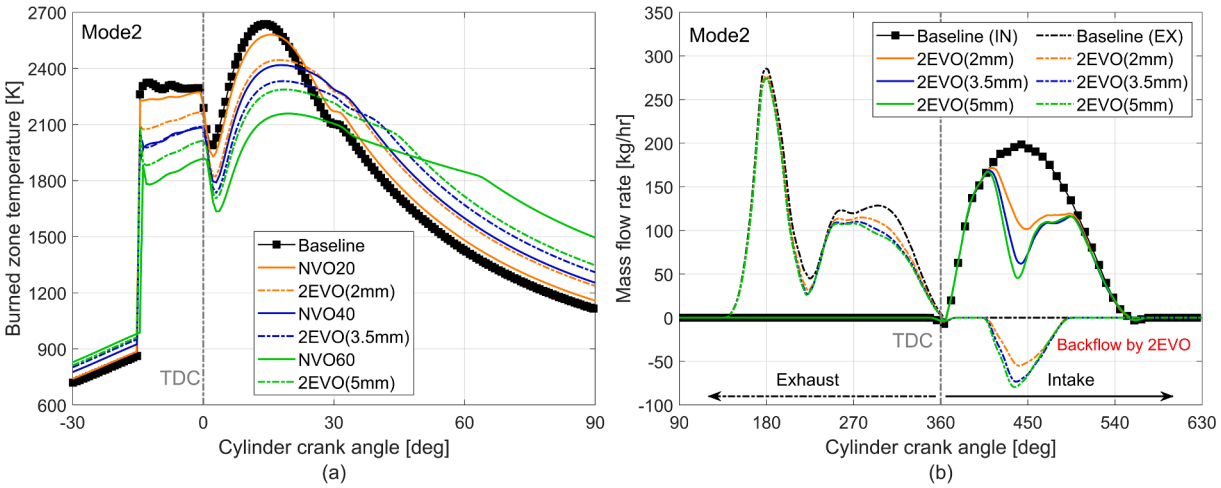

Fig. 18. Simulation results of NVO and 2EVO at Mode2: (a) burned zone temperature; and (b) instantaneous mass flow rate via intake and exhaust valves.

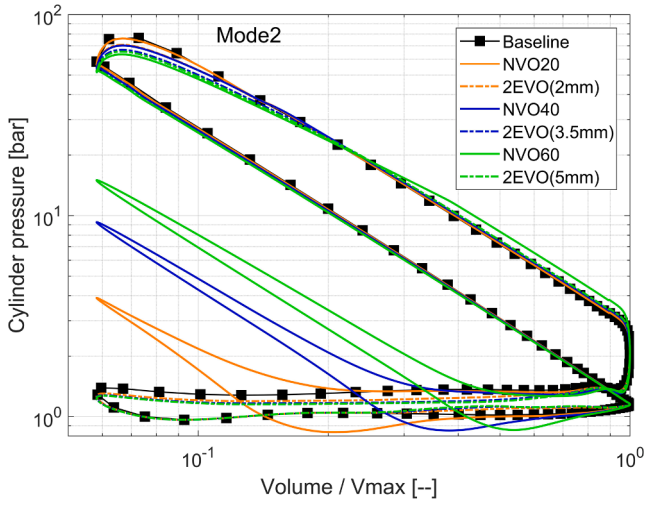

Fig. 19. Simulation results of log P – log V diagram from NVO and 2EVO at Mode2.

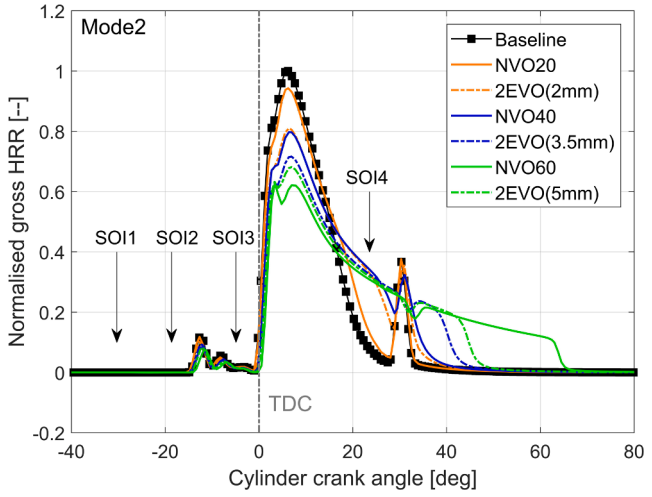

Fig. 20. Simulation results of NVO and 2EVO at Mode2: normalised gross HRR.

The reduced intensity of premixed combustion in both NVO and 2EVO with increasing EGR resulted from less excess oxygen. Introducing hot exhaust gases when injection was initiated does not reduce in-cylinder mixture temperature, so ignition delay time or mixing time was not affected negatively, unlike intake modulation. However, less oxygen concentration with EGR yielded poor air–fuel mixing and less premixed charge. This reduced premixed combustion. The lower HRR in premixed combustion reduced the peak cylinder pressure and lowered peak combustion temperature, as shown in Fig. 18(a). Although both intake modulation and i-EGR exhibited similar cylinder-pressure profile trends, their differing ignition delays caused hugely different combustion behaviour.

NVO and 2EVO show similar emission trends in Fig. 21. These are typical of diesel engines with EGR. First, Fig. 21(a) shows huge NO_x reduction (up to ~ −99 %) with increasing EGR, due to the reduction in peak combustion temperature, as seen in Fig. 18(a). However, other emissions rose. Fig. 21(b) shows soot was increased by up to +145 %. The air–fuel mixture became rich due to reduced excess air, as seen in Fig. 17(f), promoting soot formation. Also, the lower flame temperature and less excess oxygen reduced the rate of soot oxidation/re-burning [56]. HC and CO emissions increased by up to +239 % and +107 % respectively, as shown in Fig. 21(c) and (d). These are the results of increased incomplete combustion, stemming from poor air–fuel mixing with high EGR rates. Additionally, the low oxygen concentration suppressed oxidation, contributing to increasing carbon emissions. NVO60 had the highest EGR effect and also recorded most of the highest soot, HC and CO emissions.

Internal EGRs dilution effect has demonstrated the capability to raise EGT by more than +200 °C. Increasing the EGR fraction raises EGT by restricting in-cylinder air mass, thus lowering heat capacity. However, this huge improvement in EGT is accompanied by a considerable BSFC penalty, because EGR harms combustion. This penalty can be mitigated to some extent by adjusting injection timing. EGR suppresses NO_x by up to 99 %, but the rich mixture increases other emissions.

3.5. *Effect of cylinder deactivation (CDA) and cylinder cut-out (CCO)*

Fig. 22 illustrates how CDA and CCO affect EGT and IAF over different boost pressure levels. The model gradually varied boost pressure, as shown in Fig. 22(a). The same boost pressure was imposed in both CDA and CCO operation at each boost level (v1, v2, and v3) except Mode2 (boost v3), where the turbocharger could not deliver the target boost. Fig. 22(b) shows CDA enhanced EGT up to +264 °C (boost v1) from its baseline, whereas CCO raised EGT by only +101 °C (boost v1). Despite this difference in EGT increment, both strategies have high

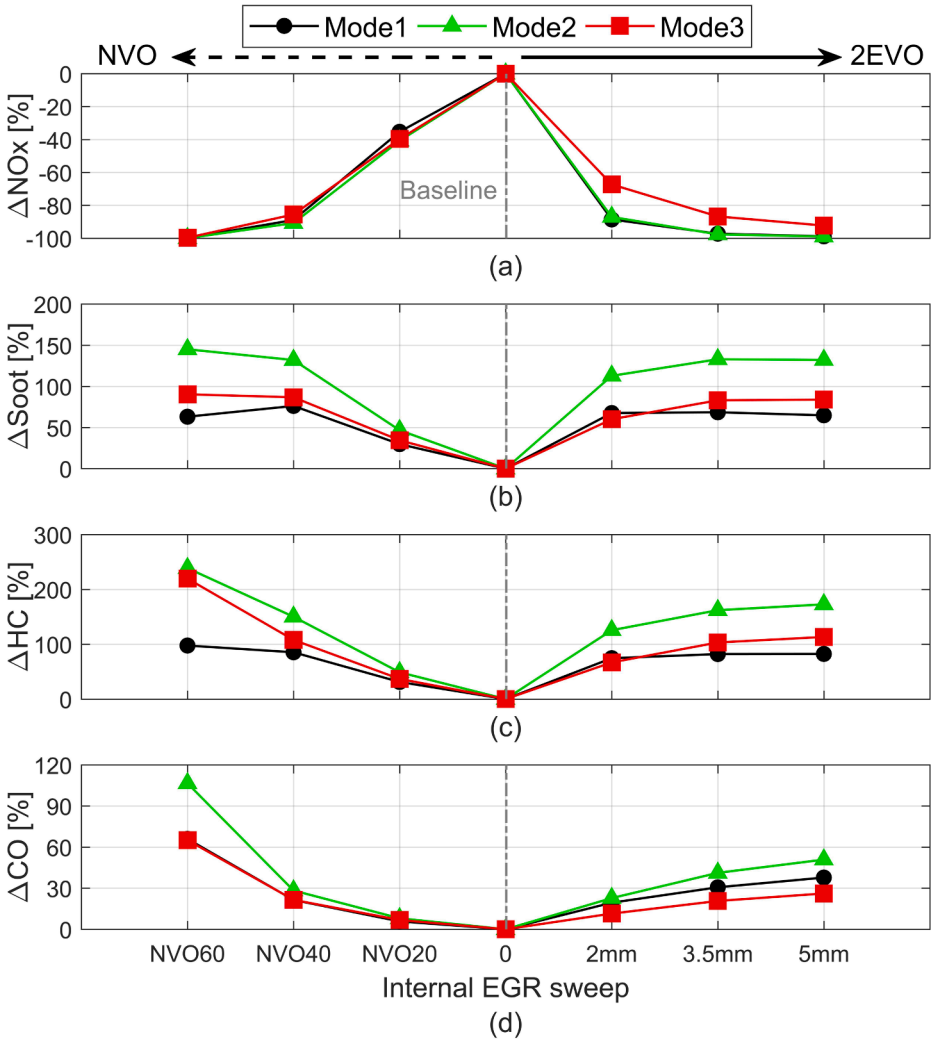

Fig. 21. Simulation results of engine-out emissions from NVO and 2EVO: (a) ΔNO_x; (b) ΔSoot; (c) ΔHC; and (d) ΔCO.

overall combustion temperature compared to baseline at Mode1, as seen in Fig. 23(a). The same trend was observed at other operating points. This is explained later.

The primary effect of high combustion temperature is increased HRR, as shown in Fig. 23(b). Since the two deactivated cylinders did not produce any work, the activated cylinders need to work almost twice as hard to maintain the same performance, as seen in Fig. 24(c). Hence, more fuel was injected, raising combustion temperature compared to the baseline, as shown in Fig. 23(a).

The secondary effect is boost pressure. Increasing boost pressure with both CDA and COO reduced EGT. This is associated with the heat capacity effect, as discussed before. Increasing boost pressure delivered more air into the activated cylinders, as observed in Fig. 22(c). This increased the heat capacity, which suppressed high temperature increment during combustion. For this reason, the high boost pressure showed lower combustion temperature after 30 CAD from TDC in Fig. 23 (a), leading to lower EGT. However, it was observed that the primary effect is much stronger than the secondary effect in the present study.

It was noted above that CDA and CCO produced broadly similar combustion temperatures, but that CDA obtained an EGT that was more than +100 °C higher than CCO. This is mainly due to the different gas exchange process arising from different valve motions in the deactivated cylinders. Fig. 25 illustrates contour plots of temperature along the exhaust pipe lines at Mode1 (boost v3). CCO allowed the deactivated cylinders to breathe as usual, but because combustion did not occur, they discharged rather cold charges, as shown in Fig. 25(a). The mixing of the cold charges with hot gases from activated cylinders meant a large amount of thermal energy was lost, restricting the EGT increment. In fact, the impact of CCÓs cold gases could even reduce EGT below the baseline level at Mode2, as seen in Fig. 22(b).

In contrast, all valves were shut down in CDÁs deactivated cylinders, so there was no mixing, as shown in Fig. 25(b). Instead, some hot gases flowed back to the exhaust line of deactivated cylinders, heating up the exhaust pipe. Even though there are some losses during backflow, it is not that significant compared to CCO. This contributed to maintaining a high EGT in CDA. This demonstrates that the valve operation of deactivated cylinders strongly affects EGT. Since the charges were not equally distributed in CDA, the total air mass flow in Fig. 22(d) could not provide correct in-cylinder air mass distribution. Instead, net charge flow per activated cylinder is a more useful parameter to estimate heat capacity effect.

Furthermore, differences in the gas exchange process in the deactivated cylinders have different impact on fuel efficiency, as seen in Fig. 24(a). CCO showed a high BSFC penalty of up to 15 % against the baseline (boost v1 at Mode3), whereas CDÁs penalty was no greater than +2.9 % (boost v1 at Mode1). CDA even displayed better BSFC than the baseline at some points with high boost pressure. Fig. 24(b) indicates that CCÓs larger fuel penalty stemmed mainly from its higher pumping work. To investigate the factors that induce a large pumping work, Fig. 26 compares PMEP in both activated and deactivated cylinders

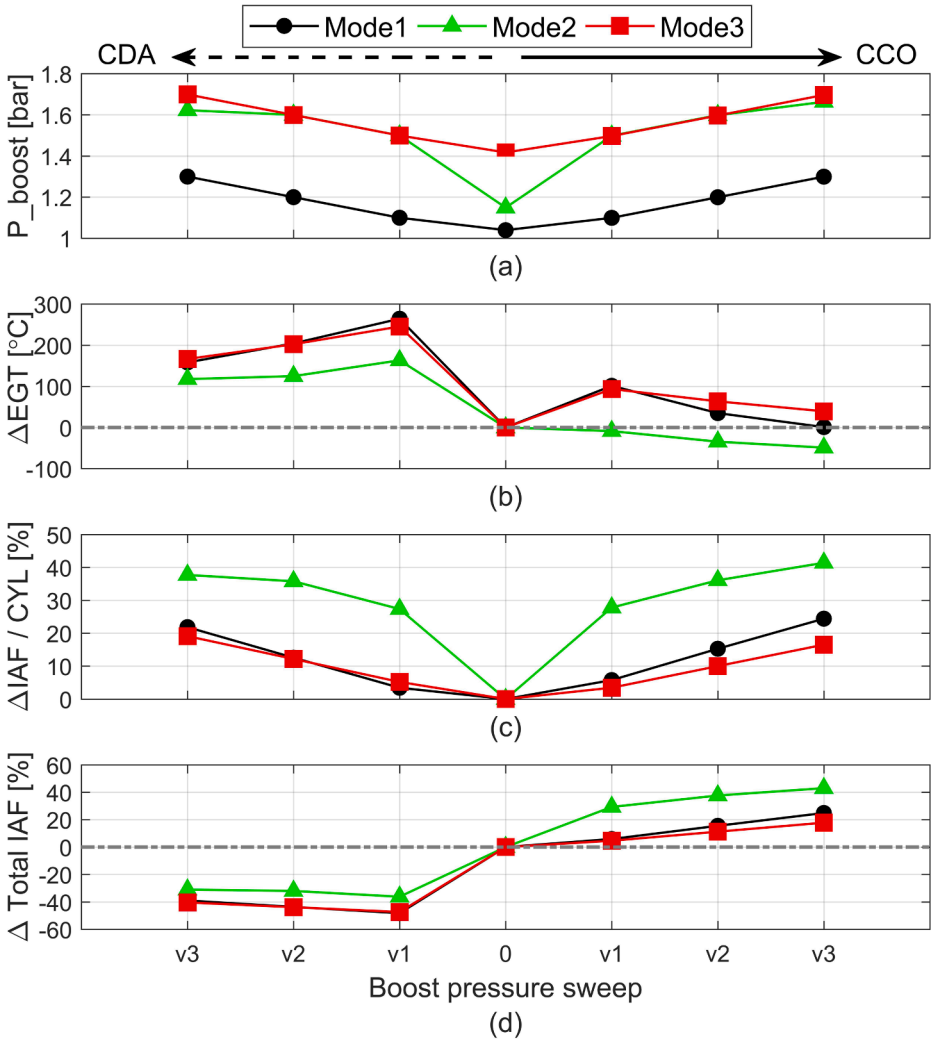

Fig. 22. Simulation results of CDA and CCO: (a) boost pressure; (b) ΔEGT; (c) ΔIAF per activated cylinder; and (d) Δtotal IAF.

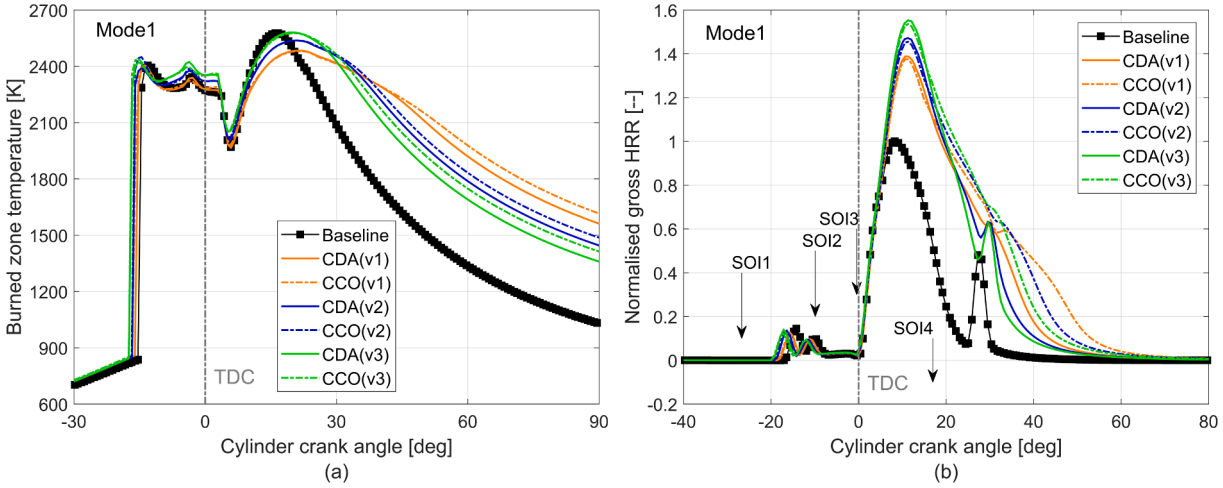

Fig. 23. Simulation results of CDA and CCO at Mode1: (a) burned zone temperature; and (b) normalised gross HRR.

(CYL_a/CYL_d) with average values (AVG) at boost v2, showing that high pumping work in both CCO's activated and deactivated cylinders mostly.

The high PMEP in the activated cylinder is likely from high back pressure due to over-closed wastegate because CCO has rather low exhaust enthalpy at turbine inlet suffering from low EGT (Fig. 22b). However, the opening of the waste-gate cannot be traced back due to the encryption of the turbocharger model in the present study. This effect was rather small at Mode1 owing to rather low boost requirement. However, it was more severe at Mode2/3 when boost control was

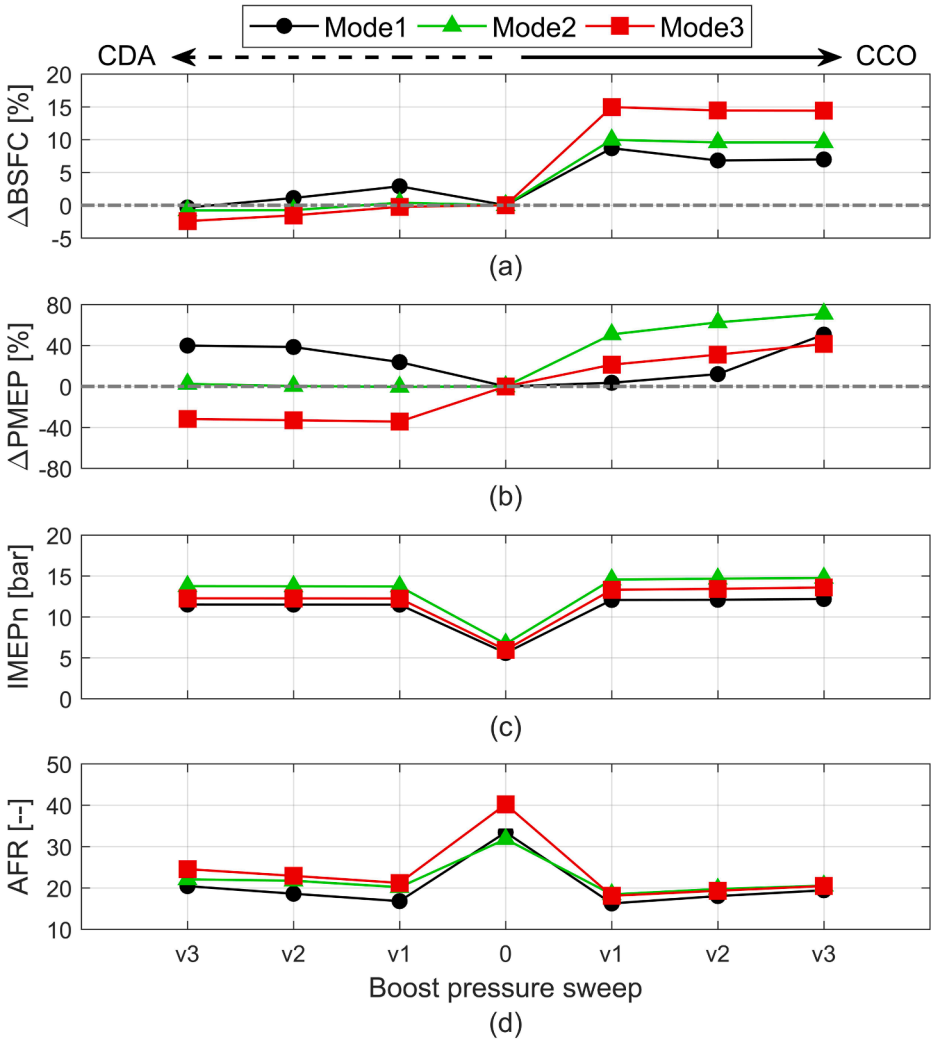

Fig. 24. Simulation results of CDA and CCO: (a) ΔBSFC; (b) ΔPMEP; (c) Δnet IMEP; and (d) AFR in activated cylinder.

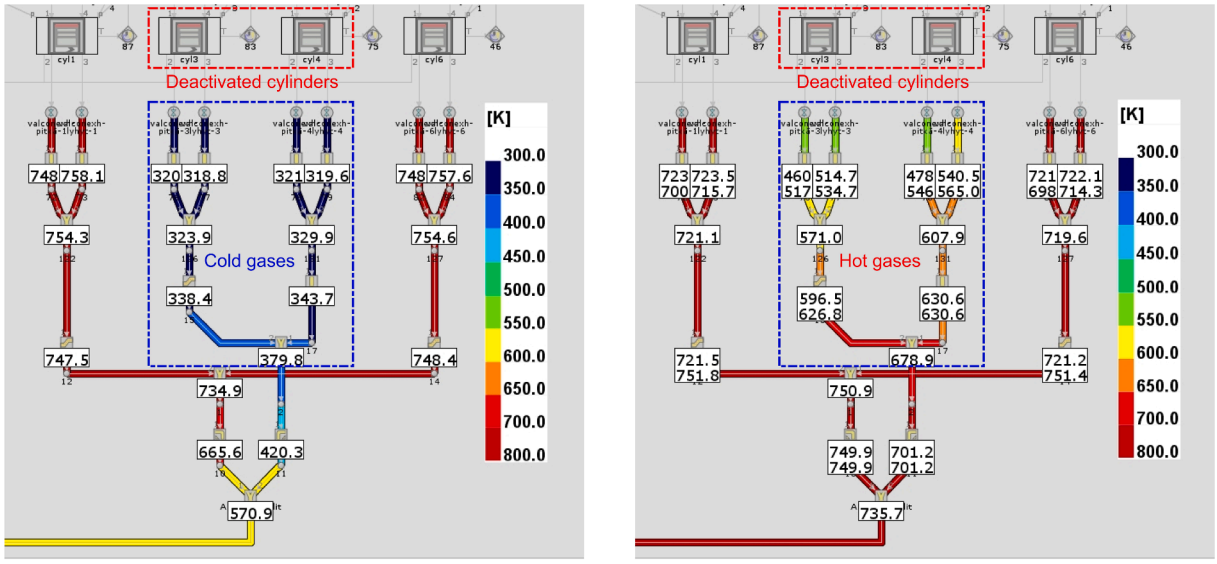

Fig. 25. Contour plot of exhaust temperature at Mode1 (boost v3): (a) CCO; and (b) CDA.

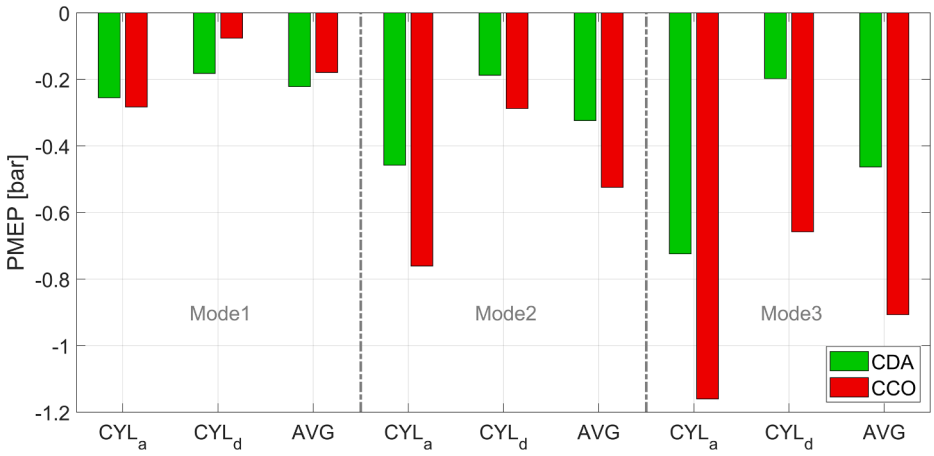

Fig. 26. Comparison of PMEP in activated and deactivated cylinders for CDA and CCO at Mode1, Mode2 and Mode3 (boost v2).

actively involved with increased boost pressure. Even though CDA increased averaged PMEP up to 40 % at Mode1 (Fig. 24b), this increment is very small as seen in Fig. 26.

The high pumping work in the deactivated cylinders is attributed to normal valve operation. Fig. 27 presents P-V diagram of a deactivated cylinder in log scale for both cases at Mode3. It clearly shows that CCO has large pumping loop due to normal valve operation. However, CDA had no pumping loop because valve operation was not involved. In a similar manner, it became severe at Mode2/3 in Fig. 26 due to high back pressure with wastegate control while CCO's PMEP at Mode1, was less affected due to low boost demand. It is noteworthy that boost control could influence the gas exchange process and pumping loop to some extent in CDA/CCO. Consequently, CCO incurred a higher fuel penalty because it needs to produce more work to compensate for pumping losses in both activated and deactivated cylinders except Mode1. This explains why CCÓs IMEP is slightly higher than CDÁs in Fig. 24(c).

Another interesting trend is that increasing boost pressure could reduce the BSFC penalty. This relates to combustion behaviour. Fig. 23 (b) shows ignition delay was short due to the high in-cylinder temperature derived from increased engine load. Premixed combustion was enhanced in both CDA and CCO with increasing boost pressure, because this delivered more air which improved air–fuel mixing and the amount of premixed charge. Even though ignition delay was slightly shorter, premixed combustion was enhanced by the abundant excess air from increased boost pressure. The extra premixed combustion at high boost pressure released more heat, raising peak combustion temperature, and advanced the combustion phase as shown in Fig. 23(b). Since more fuel burned earlier near TDC, this promoted more effective work transfer. Consequently, BSFC at high boost pressure (v3) was reduced by up to −3.2 % (CDA) and −1.7 % (CCO) compared to low boost pressure (v1). BSFC could be improved even further by optimising injection timing to achieve the same MFB50 as the baseline.

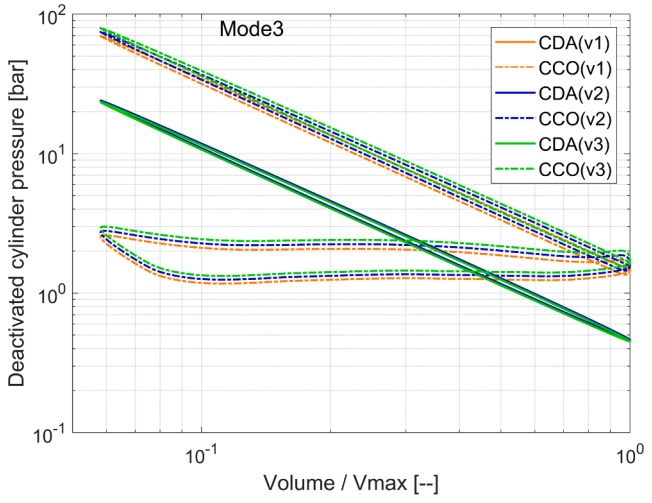

Fig. 27. Simulation results of CDA and CCO: log P – log V diagram of deactivated cylinder at Mode3.

Fig. 23(b) shows that combustion was longer and slower with CDA and CCO compared with the baseline. This is mainly due to a longer main fuel injection duration. Injection pressure and start of injection (SOI) were fixed, so injection duration needs to be extended to deliver more fuel. This lengthened the whole combustion process. In practice, injection pressure is supposed to be increased with increased engine load in CDA and CCO, but this was not considered in the present study. Raising the injection pressure would reduce the long combustion duration to some extent. CCÓs combustion duration was slightly longer than CDÁs at all three boost levels, since CCO needed increased fuelling and hence had a longer main fuel injection duration. Combustion duration was shorter at high boost pressure because increased premixed combustion burned more fuel at the early stage of the combustion.

Fig. 28 depicts engine-out emissions, and shows that both CDA and CCO display similar trends with increasing boost pressure. Fig. 28(a) shows that raising boost pressure also increases NO_x emission. This is a consequence of increased peak combustion temperature due to enhanced premixed combustion releasing more heat at the beginning of combustion. However, note that NO_x emission was reduced by 50 % at low boost pressure (v1) for both CDA and CCO because their peak combustion temperature was lower than the baselinés, as seen in Fig. 23 (a). This mainly is due to maintained injection pressure, despite increased load. In real-world operation, higher peak combustion temperature is expected with increasing injection pressure with CDA and CCO. But even though this means engine-out NO_x emission would be higher, the increased EGT will enhance EATS efficiency, so tailpipe NO_x emissions will be lower.

Soot, HC and CO emissions were increased by cutting half of the cylinders (boost v1), as seen in Fig. 28(b), (c), and (d). The increased main fuel injection quantity created locally rich mixture, as seen in Fig. 24(d), causing high soot formation. Fuel injection was more than doubled in the activated cylinders; there was insufficient excess air to be mixed completely, resulting in incomplete combustion. Higher boost pressure provided more excess air, promoting better air–fuel mixing and alleviating locally rich mixture. This suppressed formation of soot, HC and CO but also lowered EGT. Additionally, increased oxygen concentration encouraged more oxidation. But these emissions never fell below their baseline levels, since formation was still greater than oxidation, except in the case of CO emission at CDA operation. However, several experimental studies have demonstrated that soot, HC and CO emissions

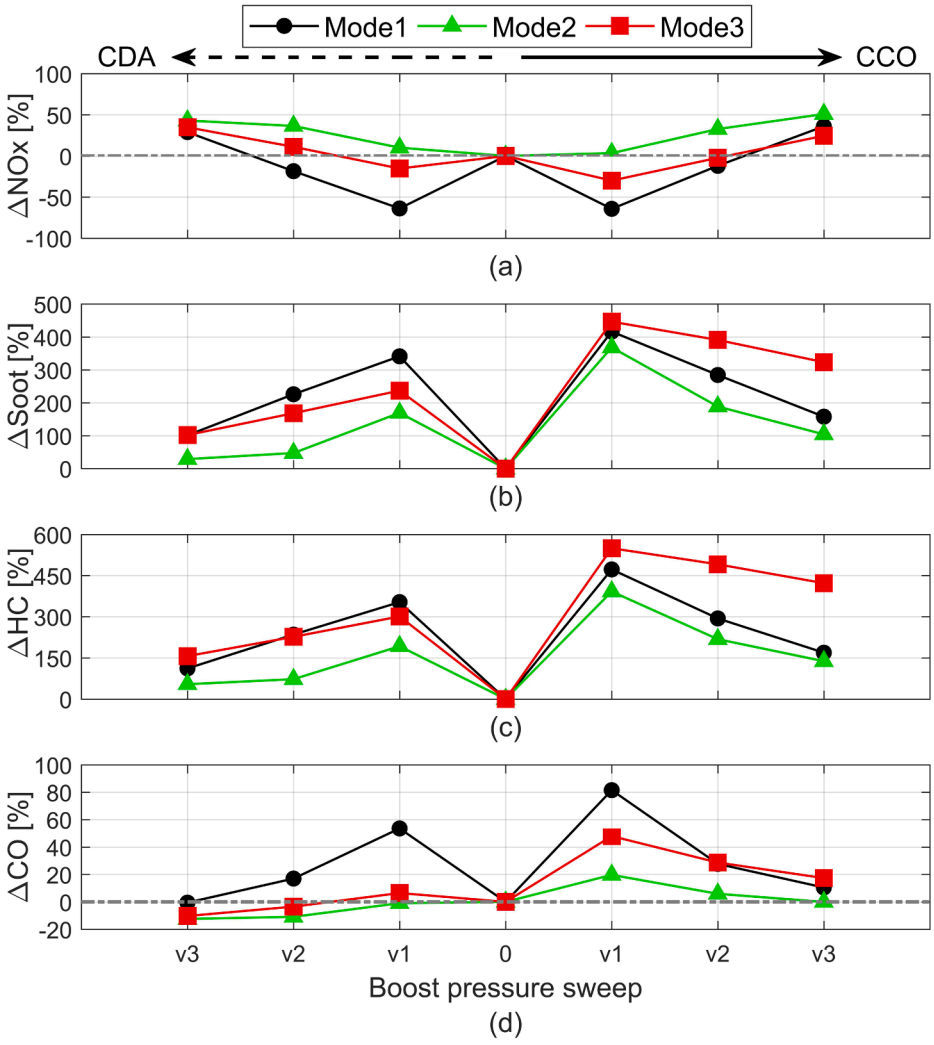

Fig. 28. Simulation results of engine-out emissions from CDA and CCO: (a) ΔNO_x; (b) ΔSoot; c) ΔHC; and (d) ΔCO.

can be cut by more than 50 % in CDA and CCO by increased oxidation, high air fuel ratio (AFR) and increased injection pressure [57,58].

Both CDA and CCO improved EGT, mainly by increased heat release in activated cylinders. CDA achieved extremely high EGT increment of more than +250 °C, with only a minor BSFC penalty (<2.5 %). CCO gave an EGT increment of up to +101 °C, but with a BSFC penalty of up to 15 %. Both generated similar in-cylinder thermal conditions under same boost pressure, but the differing valve profile in deactivated cylinders caused different outcomes for EGT, BSFC and emissions, due to the mixing effect. Raising boost pressure could improve BSFC and emissions (soot, HC and CO) to some extent, but reduces the EGT benefits. However, the maximum achievable boost level is limited by the characteristics of turbocharger. Despite of noise, vibration and harshness arising from unbalanced cylinder firing in CDA and CCO, it can be effectively

Table 5
Summary of VVA impact on ΔEGT; ΔIAF; ΔBSFC; ΔPMEP; combustion; and engine-out emissions.

Category	VVA	ΔEGT	ΔIAF	ΔBSFC	ΔPMEP	Combustion effect	EGT control mechanism	ΔNO_x	ΔSoot	ΔHC	ΔCO
Intake modulation	EIVC	++	–	+	–	More premixed	Air flow reduction	—	+	+	++
	LIVC	++	–	-+	–	combustion	(low heat capacity)	–	+	+	+
Exhaust modulation	EEVO	+	-+	+++	+	No major effect	Combustion duration	+	++	++++	–
	LEVO	+	-+	+++	+++			+	+	+	+
Internal EGR	NVO	++	–	+++	++	Less premixed	Air flow reduction	—	++	+++	++
	2EVO	+	–	+	–	combustion	(low heat capacity)	—	++	+++	+
Cylinder deactivation	CDA	+++	–	-+	–		Increased heat	–	+++	+++	+
	CCO	+	–	++	+		release	–	++++	++++	+

ΔEGT (+: increased temperature; –: decreased temperature) ΔIAF (+: increased mass flow; –: decreased mass flow).
ΔBSFC (+: deteriorated or increased fuel consumption; –: improved or reduced fuel consumption) ΔPMEP (+: increased pumping work; -: decreased pumping work).
ΔNO_x / ΔSoot / ΔHC / ΔCO (+: deteriorated or increased emissions; –: improved or reduced emissions).
ΔEGT: + < 100 °C, 100 °C <++<150 °C, 200 °C <+++, ΔIAF: –<-30 %, −30 %<-<-1%, −1%<-+<+1%.
ΔBSFC: −1%<-+<+1%, +1%<+<+5%, +5%<++<+10 %, +10 %<+++, ΔPMEP: −50 %<–<-10 %, −10 %<-<0%, 0 %<+<+50 %, +50 %<++<+150 % +150 %< +++.
ΔEmissions: —<-90 %, −90 %<–<-50 %, −50 %<-<0%, 0 %<+<+50 %, +50 %<++<100 %, +100 %<+++<+400 %, +400 %<++++.

mitigated in diesel engines [59,60]. Equally, it has been demonstrated that smooth transient performance can be achieved without severe torque variations during the switching phase [61,62].

3.6. Comparison of all VVA strategies

All VVA strategies have been evaluated at the same operating points under constant load conditions, enabling direct compassion. Table 5 summarises the case-averaged effects of VVA on EGT, IAF, BSFC, PMEP, combustion and emissions. Additionally, Fig. 29 illustrates EGT-BSFC performance. These graphs highlight common characteristics. First, all VVA strategies indicate potential to increase EGT above the baseline, with the exception of CCO at Mode2, where EGT declined. Second, increasing EGT is always accompanied by increasing fuel penalty, regardless of engine operating point, but again with one exception: intake modulation at Mode3 showed better BSFC than baseline. In general, the fuel penalty is mainly associated with either high pumping work or degraded combustion, or a combination of both. Optimising combustion parameters can minimise the fuel penalty stemming from deterioration of combustion. In contrast, it is rather difficult to reduce pumping work, since it is determined by valve timing and profiles as well as turbocharger control. Nevertheless, combustion proved to be the dominant effect on BSFC in the present study, so optimising the combustion phase remains a viable option for minimising the BSFC penalty to some extent.

Fig. 29 shows the general trend of a trade-off between EGT and BSFC, with a few exceptions. Real-world implementation demands that the most fuel-efficient options are considered. Fig. 29's plots can be divided into two sub-regions to evaluate VVA strategy in terms of fuel efficiency. The ideal strategy will be located near the top left corner, indicating simultaneous high EGT increment and low BSFC penalty. This points to cylinder deactivation as our study's most fuel-efficient strategy, since it elevated EGT by more than +250 °C, even with lower BSFC than the baseline. It is followed by intake modulation, with high potential of EGT increment above +150 °C and a minor fuel penalty of up to +3.5 %. The low BSFC penalty in both cases stems from low pumping work. Table 5 shows that intake modulation also has the benefit of a relatively low emissions penalty compared to others. However, both strategies have further potential to reduce their BSFC penalty by optimisation, which was outside the scope of this study. Therefore, cylinder deactivation and intake modulation emerge as promising solutions for efficient exhaust thermal management.

Poorer strategies are near the bottom right corner of Fig. 29, where EGT increment is rather low, but fuel penalty is excessive. Cylinder cut-out and exhaust modulation proved to be extremely inefficient in this study, with fuel efficiency deterioration of more than +15 % for an EGT elevation of no more than +100 °C above baseline. Hence, they should be avoided. Their poor fuel efficiency is due mainly to high pumping losses, indicating that the gas exchange process affected by VVA plays an important role in fuel efficiency. Suppressing their high fuel penalty would entail comprising their EGT increment by avoiding extreme valve modulation. This is applicable to all strategies. However, the latest research has demonstrated significant reduction of pumping loss in CCO is attainable by partial breathing of non-fired cylinders: this leads to similar EGT-BSFC performance as CDA [63]. The present study applied only one VVA strategy at a time, but others have demonstrated a combination of more than two VVA strategies could minimise the BSFC penalty and maximise EGT [29,33,64,65].

The most promising VVA strategies revealed by this study are to be subjected to experimental verification in follow-up work. The simulation activities continue towards model-based co-optimisation of different strategies, and extending into advanced combustion concepts such as low temperature combustion.

4. Conclusions

This study investigated all promising VVA strategies (intake modulation, exhaust modulation, internal EGR, cylinder deactivation and cylinder cut-out) to evaluate their potential for efficient exhaust thermal management at low-load conditions. Notably, such a comprehensive analysis has not been conducted for a state-of-the-art off-road engine platform in any other published study to date. The combination of cutting-edge model-based investigations and meticulously conducted validation experiments provides significantly greater insight than afforded by standalone engine testing in prior works. The key findings improve the fundamental understanding of VVA's mechanisms and their interaction. The results support the assertion that it is feasible for the next generation of engines for non-road mobile applications to meet the substantially tightened emission limits anticipated by the EPA Tier 5 legislation. These findings can be summarised as follows:

- All strategies supported by a fully-flexible VVA system have a positive effect on increasing EGT, but fuel efficiency and emissions are mostly negatively affected (trade-off).
- The most efficient VVA strategies are CDA and intake modulation. Both could elevate EGT by more than +150 °C, facilitating efficient catalytic conversion, with minor negative or positive effect on fuel consumption.
- CDA has the best EGT/efficiency ratio. Under challenging conditions of high engine-speeds and low loads, where achieving high conversion rates is particularly difficult, one can simultaneously improve the fuel economy by 2.5 % while achieving EGT increment of 166 °C. Alternatively, adjusting waste-gate settings, gives as much as 245 °C elevation in EGT with statistically same engine efficiency.

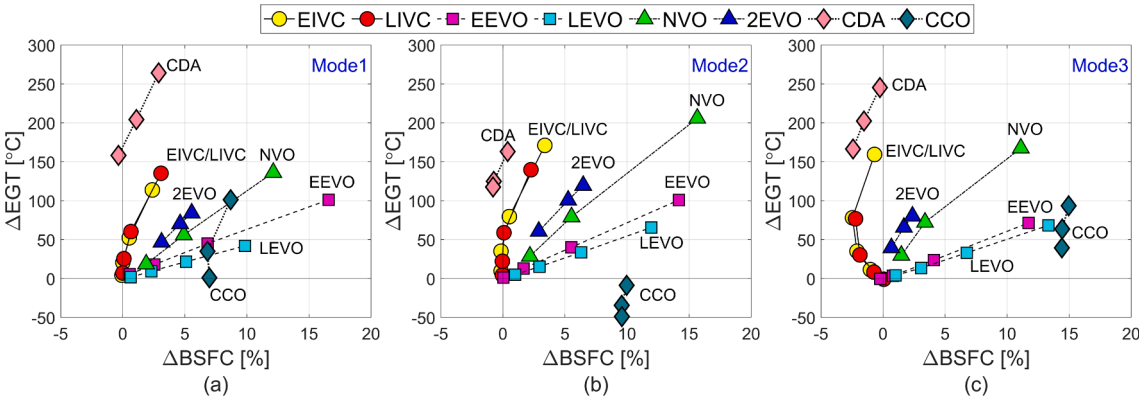

Fig. 29. EGT-BSFC performance: (a) Mode1; (b) Mode2; and (c) Mode3.

- The most inefficient strategies are exhaust modulation and cylinder cut-out. A high fuel penalty of up to +16.5 % was observed but EGT increment was below 100 °C and even can be lower than baseline.
- EGT increment is achieved mainly by three mechanisms: reduction of in-cylinder trapped air mass (intake modulation and internal EGR); increased heat release rate (CDA and CCO); and change of combustion duration (exhaust modulation).
- BSFC penalty is attributed to inefficient gas exchange process (high pumping work) and ineffective work transfer by shifted combustion phase.
- VVA affects combustion characteristics such as ignition delay, premixed combustion and combustion phase by changing in-cylinder mixture conditions. However, combustion can be corrected or optimised by altering fuel injection timing or by other methods, such as external EGR. This could minimise BSFC penalty.
- VVA generally produces more engine-out emissions such as soot, HC, and CO with increasing EGT due to a rich mixture. However, the higher EGT is expected to accelerate catalytic reaction and so reduce tailpipe emissions. Moreover, the formation of engine-out emissions can be suppressed by increasing air–fuel ratio and injection pressure.
- Intake modulation excels in this regard, demonstrating significant engine-out NO_x reduction (>90 %) and minimal adverse effects on carbon emissions (HC, CO, and soot), all while maintaining excellent thermal and performance results.

CRediT authorship contribution statement

Jeyoung Kim: Writing – review & editing, Writing – original draft, Visualization, Validation, Software, Methodology, Investigation, Formal analysis, Data curation, Conceptualization. **Marko Vallinmaki:** Software, Resources, Methodology. **Tino Tuominen:** Validation, Resources. **Maciej Mikulski:** Writing – review & editing, Supervision, Funding acquisition.

Declaration of competing interest

The authors declare that they have no known competing financial interests or personal relationships that could have appeared to influence the work reported in this paper.

Data availability

The data that has been used is confidential.

Acknowledgements

This research was conducted in the Clean Propulsion Technologies project, funded by Business Finland, Finland (ref. 38485/31/2020). The authors would like to thank Tino Tuominen, Mårten Westerholm, Sami Nyyssönen, Christer Söderström, Ari-Pekka Pellikka and Petri Söderena from VTT Technical Research Centre of Finland for performing engine tests and sharing experimental data. Thanks go also to Marko Vallinmaki and Pekka Nousiainen from AGCO Power for sharing the engine model and technical support on model modification and engine simulation. Lastly, thanks to David Wilcox for proofreading the manuscript.

References

[1] D.B. Gosala, A.K. Ramesh, C.M. Allen, M.C. Joshi, A.H. Taylor, M.V. Voorhis, G. M. Shaver, L. Farrell, E. Koeberlein, J. McCarthy Jr., D. Stretch, Diesel engine aftertreatment warm-up through early exhaust valve opening and internal exhaust gas recirculation during idle operation, Int. J. Engine Res. 19 (7) (2018) 758–773, https://doi.org/10.1177/1468087417730240.

[2] H. Fang, Challenges with the ultimate energy density with li-ion batteries, IOP Conf. Ser.: Earth Environ. Sci. 781 (2021), https://doi.org/10.1088/1755-1315/781/4/042023.

[3] D.B. Gosala, C.M. Allen, A.K. Ramesh, G.M. Shaver, J. McCarthy Jr., D. Stretch, E. Koeberlein, L. Farrell, Cylinder deactivation during dynamic diesel engine operation, Int. J. Engine Res. 18 (10) (2017) 991–1004, https://doi.org/10.1177/1468087417694000.

[4] X. Li, H. Gao, L. Zhao, Z. Zhang, X. He, F. Liu, Combustion and emission performance of a split injection diesel engine in a double swirl combustion system, Energy 114 (Nov. 2016) 1135–1146, https://doi.org/10.1016/j.energy.2016.08.092.

[5] B. Wang, Autoignition of light naphtha and its surrogates in a rapid compression machine, Energy Sci. Eng. 7 (1) (Feb. 2019) 207–216, https://doi.org/10.1002/ese3.270.

[6] B.G. Jeong, J.H. Won, K.C. Oh, H.S. Heo, S. Bae, H.J. Seo, H. Kim, Characteristics of integrated air control and low-pressure exhaust gas recirculation valve for diesel engines, Int. J. Automot. Technol. 21 (1) (2020) 239–247, https://doi.org/10.1007/s12239-020-0023-x.

[7] Y. Liang, X. Ding, J. Dai, M. Zhao, L. Zhong, J. Wang, Y. Chen, Active oxygen-promoted NO catalytic on monolithic Pt-based diesel oxidation catalyst modified with Ce, Catal. Today 327 (2019), https://doi.org/10.1016/j.cattod.2018.06.008.

[8] C. Guardiola, B. Pla, J. Mora Pérez, D. Lefebvre, Experimental determination and modelling of the diesel oxidation catalysts ageing effects, Proceedings of the Institution of Mechanical Engineers, Part D: Journal of Automobile Engineering 233 (12) (Oct. 2019) 3016–3029, https://doi.org/10.1177/0954407018814305.

[9] B. Pla, P. Piqueras, P. Bares, A. Aronis, Simultaneous NOx and NH3 slip prediction in a SCR catalyst under real driving conditions including potential urea injection failures, Int. J. Engine Res. 23 (7) (Jul. 2022) 1213–1225, https://doi.org/10.1177/14680874211007646.

[10] H. Zhang, J. Wang, Ammonia coverage ratio and input simultaneous estimation in ground vehicle selective catalytic reduction (SCR) systems, J. Franklin Inst. 352 (2) (Feb. 2015) 708–723, https://doi.org/10.1016/j.jfranklin.2014.06.009.

[11] A. Ko, Y. Woo, J. Jang, Y. Jung, Y. Pyo, H. Jo, O. Lim, Y.J. Lee, Complementary effects between NO oxidation of DPF and NO2 decomposition of SCR in light-duty diesel engine, J. Ind. Eng. Chem. 80 (Dec. 2019) 160–170, https://doi.org/10.1016/j.jiec.2019.07.045.

[12] P. Jiao, Z. Li, B. Shen, W. Zhang, X. Kong, R. Jiang, Research of DPF regeneration with NOx-PM coupled chemical reaction, Appl. Therm. Eng. 110 (Jan. 2017) 737–745, https://doi.org/10.1016/j.applthermaleng.2016.08.184.

[13] A. García, J. Monsalve-Serrano, D. Villalta, R. Lago Sari, Performance of a conventional diesel aftertreatment system used in a medium-duty multi-cylinder dual-mode dual-fuel engine, Energy Conv. Manag. 184 (Mar. 2019) 327–337, https://doi.org/10.1016/j.enconman.2019.01.069.

[14] K. Lee, J. Lee, S. Lee, K. Oh, S. Jang, Fuel Consumption and Emission Reduction for Non-Road Diesel Engines with Electrically Heated Catalysts, Catal. 13 (6) (2023), https://doi.org/10.3390/catal13060950.

[15] Y.M. López - De Jesús, P.I. Chigada, T.C. Watling, K. Arulraj, A. Thorén, N. Greenham, P. Markatou, NOx and PM Reduction from Diesel Exhaust Using Vanadia SCRF®, SAE Int. J. Engines 9 (2) (2016) https://doi.org/10.4271/2016-01-0914.

[16] Volkswagen, Clean and cultivated: the 2.0 TDI engine with new Euro 6d emission standard (2020). https://www.volkswagen-newsroom.com/en/press-releases/clean-and-cultivated-the-20-tdi-engine-with-new-euro-6d-emission-standard-6721. (Accessed 11 Sep 2023).

[17] BOSCH, Exhaust-gas treatment with double-injection (2019). https://www.bosch-mobility.com/en/solutions/exhaust-gas-treatment/exhaust-gas-treatment-with-double-injection-technology. (Accessed 11 Sep 2023).

[18] Y. Zhu, W. Zhou, C. Xia, Q. Hou, Application and Development of Selective Catalytic Reduction Technology for Marine Low-Speed Diesel Engine: Trade-Off among High Sulfur Fuel, High Thermal Efficiency, and Low Pollution Emission, Atmosphere 13 (5) (2022), https://doi.org/10.3390/atmos13050731.

[19] Y. Zhang, C. Xia, D. Liu, Y. Zhu, Y. Feng, Experimental investigation of the high-pressure SCR reactor impact on a marine two-stroke diesel engine, Fuel 335 (2023) 127064, https://doi.org/10.1016/j.fuel.2022.127064.

[20] P. Tayal, Light off temperature based approach to determine diesel oxidation catalyst effectiveness level and the corresponding outlet NO and NO2 characteristics, (2014). http://docs.lib.purdue.edu/open_access_theses/694.

[21] J. Hu, J. Liao, Y. Hu, J. Lei, M. Zhang, J. Zhong, F. Yan, Z. Cai, Experimental investigation on emission characteristics of non-road diesel engine equipped with integrated DOC + CDPF + SCR aftertreatment, Fuel 305 (Dec. 2021), https://doi.org/10.1016/j.fuel.2021.121586.

[22] R. Feng, Z. Sun, G. Li, X. Hu, B. Deng, S. Xiong, The impact of thermal status on emissions of a non-road diesel engine equipped with aftertreatment system under transient operation, Case Studies in Thermal Engineering 36 (Aug. 2022), https://doi.org/10.1016/j.csite.2022.102244.

[23] Z. Meng, C. Chen, J. Li, J. Fang, J. Tan, Y. Qin, Y. Jiang, Z. Qin, W. Bai, K. Liang, Particle emission characteristics of DPF regeneration from DPF regeneration bench and diesel engine bench measurements, Fuel 262 (Feb. 2020), https://doi.org/10.1016/j.fuel.2019.116589.

[24] C. Guardiola, B. Pla, P. Bares, J. Mora, An on-board method to estimate the light-off temperature of diesel oxidation catalysts, Int. J. Engine Res. 21 (8) (Oct. 2020) 1480–1492, https://doi.org/10.1177/1468087418817965.

[25] V. Tharad, DIESEL OXIDATION CATALYST - DIESEL PARTICULATE FILTER / CATALYTIC DIESEL FILTERS (2021). https://www.linkedin.com/pulse/diesel-oxidation-catalyst-particulate-filter-catalytic-vijay-tharad. (Accessed 20 Feb 2024).

[26] R. Villamaina, I. Nova, E. Tronconi, T. Maunula, M. Keenan, Effect of the NH4NO3 addition on the low-T NH3-SCR performances of individual and combined fe- and cu-zeolite catalysts, Emiss. Control Sci. Technol. 5 (4) (2019) 290–296, https://doi.org/10.1007/s40825-019-00140-3.

[27] S. Ma, W. Gao, Z. Yang, R. Lin, X. Wang, X. Zhu, Y. Jiang, Superior Ce–Nb–Ti oxide catalysts for selective catalytic reduction of NO with NH3, J. Energy Inst. 94 (Feb. 2021) 73–84, https://doi.org/10.1016/j.joei.2020.11.001.
[28] D.W. Stanton, Systematic development of highly efficient and clean engines to meet future Commercial vehicle greenhouse gas regulations, SAE Int. J. Engines 6 (3) (Sep. 2013) 1395–1480, https://doi.org/10.4271/2013-01-2421.
[29] K.R. Vos, G.M. Shaver, M.C. Joshi, A.K. Ramesh, J. McCarthy Jr., Strategies for using valvetrain flexibility instead of exhaust manifold pressure modulation for diesel engine gas exchange and thermal management control, Int. J. Engine Res. 22 (3) (2021) 755–776, https://doi.org/10.1177/1468087419880634.
[30] S. Bai, J. Han, M. Liu, S. Qin, G. Wang, G. Li, Experimental investigation of exhaust thermal management on NOx emissions of heavy-duty diesel engine under the world Harmonized transient cycle (WHTC), Appl. Therm. Eng. 142 (July. 2018) 421–432, https://doi.org/10.1016/j.applthermaleng.2018.07.042.
[31] K. Boriboonsomsin, T. Durbin, G. Scora, K. Johnson, D. Sandez, A. Vu, Y. Jiang, A. Burnette, S. Yoon, J. Collins, Z. Dai, C. Fulper, S. Kishan, M. Sabisch, D. Jackson, Real-world exhaust temperature profiles of on-road heavy-duty diesel vehicles equipped with selective catalytic reduction, Sci. Total Environ. 634 (2018) 909–921, https://doi.org/10.1016/j.scitotenv.2018.03.362.
[32] M. Laurén, T. Karhu, M. Laivola, J. Ekman, S. Niemi, K. Spoof-Tuomi, Different methods to improve the exhaust gas temperature in modern stage V 0ff-road diesel engine over transient emission cycles, SAE Technical Papers (2020), https://doi.org/10.4271/2020-01-0903.
[33] M.E. Magee, Exhaust Thermal Management Using Cylinder Deactivation and Late Intake Valve Closing, (2014). https://docs.lib.purdue.edu/open_access_theses/214/.
[34] B. Wu, Z. Jia, Z. guo Li, G. yi Liu, X. lin Zhong, Different exhaust temperature management technologies for heavy-duty diesel engines with regard to thermal efficiency, Appl. Therm. Eng. 186 (2021) 116495, https://doi.org/10.1016/j.applthermaleng.2020.116495.
[35] T. Tomoda, T. Ogawa, H. Ohki, T. Kogo, K. Nakatani, E. Hashimoto, Improvement of diesel engine performance by variable valve train system, Int. J. Engine Res. 11 (5) (2010) 331–344, https://doi.org/10.1243/14680874JER586.
[36] F.J. Arnau, J. Martín, B. Pla, Á. Auñón, Diesel engine optimization and exhaust thermal management by means of variable valve train strategies, Int. J. Engine Res. 22 (4) (2021) 1196–1213, https://doi.org/10.1177/1468087419894804.
[37] Z. Lou, G. Zhu, Review of advancement in Variable valve actuation of internal combustion engines, Appl. Sci. 10 (4) (2020), https://doi.org/10.3390/app10041216.
[38] A. di Gaeta, C.I. Hoyos Velasco, V. Giglio, Modelling of an electro-hydraulic variable valve actuator for camless engines aimed at controlling valve lift parameters, Int. J. Control 94 (10) (2021) 2857–2873, https://doi.org/10.1080/00207179.2020.1737333.
[39] J. Kim, A. Soleimani, P. Nousiainen, M. Axelsson, M. Mikulski, Variable valve actuation for next generation marine and off-road engines - a comprehensive review oriented on meeting future emission legislation. https://ssrn.com/abstract=4760136.
[40] S. Gehrke, D. Kovács, P. Eilts, A. Rempel, P. Eckert, Investigation of VVA-based exhaust Management strategies by means of a HD single cylinder Research engine and rapid prototyping systems, SAE Int. J. Commer. Veh. 6 (1) (Apr. 2013) 47–61, https://doi.org/10.4271/2013-01-0587.
[41] W. Guan, H. Zhao, Z. Ban, T. Lin, Exploring alternative combustion control strategies for low-load exhaust gas temperature management of a heavy-duty diesel engine, Int. J. Engine Res. 20 (4) (2019) 381–392, https://doi.org/10.1177/1468087418755586.
[42] W. De Ojeda, Effect of Variable valve timing on diesel combustion Characteristics, SAE Technical Papers (Apr. 2010), https://doi.org/10.4271/2010-01-1124.
[43] X. Zhang, H. Wang, Z. Zheng, R.D. Reitz, M. Yao, Effects of late intake valve closing (LIVC) and rebreathing valve strategies on diesel engine performance and emissions at low loads, Appl. Therm. Eng. 98 (2016) 310–319, https://doi.org/10.1016/j.applthermaleng.2015.12.045.
[44] A. Wickström, Variable Valve Actuation Strategies for Exhaust Thermal Management on a HD Diesel Engine (2012). https://www.diva-portal.org/smash/record.jsf?pid=diva2%3A541747&dswid=-9603.
[45] M.C. Joshi, G.M. Shaver, K. Vos, J. McCarthy Jr., L. Farrell, Internal exhaust gas recirculation via reinduction and negative valve overlap for fuel-efficient aftertreatment thermal management at curb idle in a diesel engine, Int. J. Engine Res. 23 (3) (2022) 369–379, https://doi.org/10.1177/1468087420984590.
[46] CARB, Tier 5 Rulemaking Workshop II - Proposed Emission Standards, 2023. https://ww2.arb.ca.gov/sites/default/files/2023-10/%232%20Proposed%20Emission%20Standards-ADA-10232023.pdf. (Accessed 25 Feb 2024).
[47] G.F. Hohenberg, Advanced approaches for heat transfer calculations, SAE Technical Papers (Feb. 1979), https://doi.org/10.4271/790825.
[48] A.P. Colburn, A method of correlating forced convection heat-transfer data and a comparison with fluid friction, Int. J. Heat Mass Transf. 7 (12) (Dec. 1964) 1359–1384, https://doi.org/10.1016/0017-9310(64)90125-5.
[49] H. Hiroyasu, T. Kadota, M. Arai, Development and use of a spray combustion modeling to predict diesel engine efficiency and pollutant emissions : Part 1 combustion modeling, Bulletin of JSME 26 (214) (1983) 569–575, https://doi.org/10.1299/JSME1958.26.569.
[50] G. Technology, "GT-SUITE Engine Performance Application Manual ver 7.1," 2022.
[51] Gamma Technologies, "Engine Performance Application Manual (Version 2022)," 2022.
[52] P. Wang, Z. Hu, L. Shi, X. Tang, Y. Liu, K. Deng, Experimental investigation of the effects of miller timing on performance, energy and exergy characteristics of two-stage turbocharged marine diesel engine, Fuel 292 (Jan. 2021), https://doi.org/10.1016/j.fuel.2021.120252.
[53] D.M. Thomas, Experimental setup and testing of a Variable valve actuation enabled cam-less natural gas engine. https://doi.org/10.25394/PGS.21685760.v1.
[55] E. Garcia, V. Triantopoulos, A. Boehman, M. Taylor, J. Li, Impact of Miller Cycle Strategies on Combustion Characteristics, Emissions and Efficiency in Heavy-Duty Diesel Engines, SAE Technical Papers, (April. 2020), https://doi.org/10.4271/2020-01-1127.
[56] D. Agarwal, S. Kumar, A. Kumar, Effect of exhaust gas recirculation (EGR) on performance, emissions, deposits and durability of a constant speed compression ignition engine, Appl. Energy 88 (8) (2011) 2900–2907, https://doi.org/10.1016/j.apenergy.2011.01.066.
[57] Y. Liu, A. Kuznetsov, B. Sa, Simulation and analysis of the impact of cylinder deactivation on fuel saving and emissions of a medium-speed high-power diesel engine, Appl. Sci. 11 (16) (2021), https://doi.org/10.3390/app11167603.
[58] K.R. Vos, G.M. Shaver, A.K. Ramesh, J. McCarthy Jr., Impact of Cylinder Deactivation and Cylinder Cutout via Flexible Valve Actuation on Fuel Efficient Aftertreatment Thermal Management at Curb Idle, Front. Mech. Eng. 5 (Aug. 2019), https://doi.org/10.3389/fmech.2019.00052.
[59] T. Reinhart, A. Matheaus, C. Sharp, B. Peters, M. Pieczko, J. McCarthy Jr., Vibration and emissions quantification over key drive cycles using cylinder deactivation, Int. J. Powertrains. 9 (4) (2020) 315–344, https://doi.org/10.1504/IJPT.2020.111245.
[60] M. Pieczko, J. McCarthy, J. Hamler, Mitigating vibration for a heavy-duty diesel cylinder deactivation truck, SAE Technical Papers (2021) 1–8, https://doi.org/10.4271/2021-01-0661.
[61] D.B. Gosala, C.M. Allen, G.M. Shaver, L. Farrell, E. Koeberlein, B. Franke, D. Stretch, J. McCarthy Jr., Dynamic cylinder activation in diesel engines, Int. J. Engine Res. 20 (8–9) (2019) 849–861, https://doi.org/10.1177/1468087418779937.
[62] C.M. Allen, M.C. Joshi, D.B. Gosala, G.M. Shaver, L. Farrell, J. McCarthy Jr., Experimental assessment of diesel engine cylinder deactivation performance during low-load transient operations, Int. J. Engine Res. 22 (2) (2021) 606–615, https://doi.org/10.1177/1468087419857597.
[63] D.B. Gosala, G.M. Shaver, J. McCarthy Jr., T.P. Lutz, Fuel-efficient thermal management in diesel engines via valvetrain-enabled cylinder ventilation strategies, Int. J. Engine Res. 22 (2) (2021) 430–442, https://doi.org/10.1177/1468087419867247.
[64] K.R. Vos, G.M. Shaver, M.C. Joshi, J. McCarthy Jr., Implementing variable valve actuation on a diesel engine at high-speed idle operation for improved aftertreatment warm-up, Int. J. Engine Res. 21 (7) (2020) 1134–1146. https://doi.org/10.1177/1468087419880639.
[65] M.C. Joshi, Opportunities to improve aftertreatment thermal management and simplify the air handling architectures of highly efficient diesel engines incorporating valvetrain flexibility. https://doi.org/10.25394/PGS.11527854.v1.